Neurobiology of Aging 77 (2019) 128–143

Contents lists available at ScienceDirect

Neurobiology of Aging

journal homepage: www.elsevier.com/locate/neuaging

Fresh evidence for major brain gangliosides as a target for the treatment of Alzheimer's disease

Marina Dukhinova [a], Tatyana Veremeyko [a], Amanda W.Y. Yung [a], Inna S. Kuznetsova [a], Thomas Y.B. Lau [a], Ekaterina Kopeikina [a], Andrew M.L. Chan [a], Eugene D. Ponomarev [a,b,*]

[a] School of Biomedical Sciences, Faculty of Medicine, The Chinese University of Hong Kong, Shatin, New Territories, Hong Kong
[b] Kunming Institute of Zoology, Chinese University of Hong Kong Joint Laboratory of Bioresources and Molecular Research of Common Diseases, Kunmin-Hong Kong, China

ARTICLE INFO

Article history:
Received 11 June 2018
Received in revised form 17 January 2019
Accepted 21 January 2019
Available online 30 January 2019

Keywords:
Alzheimer's disease
Major brain gangliosides
st3gal5
Microglia
Lectin
Neuroinflammation

ABSTRACT

Although it was suggested that gangliosides play an important role in the binding of amyloid fragments to neuronal cells, the exact role of gangliosides in Alzheimer's disease (AD) pathology remains unclear. To understand the role of gangliosides in AD pathology in vivo, we crossed st3gal5-deficient ($ST3^{-/-}$) mice that lack major brain gangliosides GM1, GD1a, GD3, GT1b, and GQ1b with 5XFAD transgenic mice that overexpress 3 mutant human amyloid proteins AP695 and 2 presenilin PS1 genes. We found that $ST3^{-/-}$ 5XFAD mice have a significantly reduced burden of amyloid depositions, low level of neuroinflammation, and did not exhibit neuronal loss or synaptic dysfunction. $ST3^{-/-}$ 5XFAD mice performed significantly better in a cognitive test than wild-type (WT) 5XFAD mice, which was comparable with WT non-transgenic mice. Treatment of WT 5XFAD mice with the sialic acid–specific *Limax flavus* agglutinin resulted in substantial improvement of AD pathology to a level of $ST3^{-/-}$ 5XFAD mice. Thus, our findings highlight an important role for gangliosides as a target for the treatment of AD.

1. Introduction

Alzheimer's disease (AD) is a systemic neurodegenerative disorder of the central nervous system (CNS) that has a high prevalence in the aging population. The disease is associated with synaptic distinction, progressive loss of neurons, brain atrophy, and progressive cognitive decline (Masters et al., 2015). An effective therapy for the disease has still not been developed (Graham et al., 2017; Selkoe and Hardy, 2016). Major hallmarks of the CNS pathology of AD include extracellular depositions of polymerized aggregated fragments of amyloid-β (Aβ) and intracellular fibrillary tangles. Polymeric and oligomeric Aβ species contribute to neuronal toxicity with subsequent neurodegeneration (Selkoe and Hardy, 2016). Neuronal amyloid precursor protein (APP) is expressed as a long transmembrane protein, which is cleaved by β-secretase and then by a γ-secretase complex consisting of 4 core proteins including presenilin (PS-1) into short peptides that stay on the cell surface (Fig. 1SA) (Selkoe and Hardy, 2016). Known mutations in human APP (hAPP) and PS-1 genes are associated with increased aggregation of amyloid fragments and earlier onset of familial AD (FAD) (Shea et al., 2016). The mouse model of AD used in the study was 5XFAD transgenic mice that overexpress under neuronal Thy1 promoter 3 mutant hAPPs and 2 mutant PS-1 genes (Fig. S1B) (Oakley et al., 2006). These mice have extracellular amyloid depositions in the brain starting at 3 months of age and represent the most severe mouse model of AD (Oakley et al., 2006). Toxic fragments of human mutant APPs (e.g., $A\beta_{1\text{-}40}$ and $A\beta_{1\text{-}42}$ peptides) are present in the CNS of 5XFAD mice and have the ability to bind to neuronal lipid rafts (NLRs) (Hicks et al., 2012; Oakley et al., 2006).

Neuronal membrane microdomains or NLRs are rigid parts of the plasma membranes of neuronal cells that are stabilized with intramembrane cholesterol and enriched with sialylated glycosphingolipids (gangliosides) and glycoproteins with sialic acid residues exposed to the surface (Fig. S1C) (Hicks et al., 2012). The areas of neuronal cells that are enriched with NLRs are postsynaptic density (PSD) membranes in neuronal synapses (Ponomarev, 2018; Suzuki et al., 2011). Gangliosides modulate the functions of receptors at postsynaptic membranes (Hollmann and Seifert, 1986; Posse de Chaves and Sipione, 2010), and the expression of gangliosides significantly changes in AD (Fukami et al., 2017). Brain tissue is specifically enriched with gangliosides referred to as major brain

* Corresponding author at: The Chinese University of Hong Kong, 323A, Lo-Kwee Seong Biomedical Sciences Building, Area 39, Shatin, New Territories, Hong Kong. Tel.: (852) 39439620; fax: (852) 2603 5139.
E-mail address: eponomarev@cuhk.edu.hk (E.D. Ponomarev).

0197-4580/$ – see front matter © 2019 Elsevier Inc. All rights reserved.
https://doi.org/10.1016/j.neurobiolaging.2019.01.020

gangliosides, including GM1, GD1a, GD1b, GT1b, and GQ1b (Sotnikov et al., 2013; Sturgill et al., 2012; Vajn et al., 2013). Gangliosides GM1, GD1a, GD1b, and GT1b account for 97% of all gangliosides in the human brain (Ando, 1983). These 4 gangliosides have the same core structure (Galβ1-3GalNAcβ1-4Galβ1-4Glcβ1-1′Cer), with one or two sialic acids attached to internal galactose in GM1 and GD1b, and an additional sialic acid on the terminal galactose of GD1a and GT1b (Yu et al., 2011b). We previously found that gangliosides GM1, GD3, GT1b, and GQ1b within NLR are recognized by platelets, leading to their degranulation and the secretion of proinflammatory factors and neurotransmitters that modulate the function of both neuronal and immune cells (Ponomarev, 2018; Sotnikov et al., 2013; Starossom et al., 2015). Gangliosides GM1 and GM2 have been shown to be accumulated in the lipid rafts AD brains (Pernber et al., 2012) and serve as a binding site for amyloid peptides, acting as a seed for Aβ aggregation (Yanagisawa, 2015). The other study showed the ganglioside loss as a primary event in AD (Svennerholm, 1994). This was confirmed by the other study where it was demonstrated that GM1 was not accumulated in absolute units, but GM1 ratio to other gangliosides was relatively increased in AD brains (Fukami et al., 2017). It was also demonstrated that inhibition of ganglioside synthesis via the inactivation of glucosylceramide synthase in neuronal cells resulted in decreased susceptibility of mouse cortical neurons to Aβ-induced toxicity (Herzer et al., 2016). However, it is currently not clear how Aβ binding to neuronal gangliosides contributes to disease pathology. The results of in vivo studies using hAPP transgenic animals that are partially deficient in certain gangliosides are contradictory. One study used 1XFAD transgenic mice that lack GM2-synthase (GM2S). These mice do not have gangliosides GM1, GD1a, GD1b, GT1b, or GQ1b but do have GD3 and GM3. Surprisingly, they have an increased amyloid plaque burden in the CNS parenchyma and brain blood vessels (Oikawa et al., 2009). This demonstrates that the remaining GD3 and GM3 gangliosides exhibit compensatory upregulation and are still capable of promoting AD pathology. Another study used 2XFAD (hAPP/PS-1) mice with knockout of GD3-synthase (GD3S). These mice lack GD1b, GD3, GT1b, and GQ1b but still have brain-abundant GM1, GD1a, and GM3 gangliosides. In contrast to GM2S-deficient 1XFAD mice, GD3S-deficient 2XFAD mice showed an amelioration of AD pathology (Bernardo et al., 2009). Thus, the exact role of GM1 and the other major brain gangliosides GD3, GT1b, and GQ1b in AD pathology remains controversial.

To understand the role of major brain gangliosides in AD pathology in vivo, we crossed 5XFAD mice with st3gal5-deficient ($ST3^{-/-}$) mice that lack GM3-synthase (α2,3-sialyltransferase), which is required for the synthesis of all major brain gangliosides (which are gangliosides of a-, b-, and c-series) in the CNS including GM1, GD1a, GD1b, GM3, GD3, GT1b, and GQ1b (Fig. S1D) (Sturgill et al., 2012; Yoshikawa et al., 2009). Thus, these mice a-, b-, and c-series ganglioside-deficient. We found that 8-month-old $ST3^{-/-}$ 5XFAD mice had a significantly lower level of amyloid plaque burden when compared with a WT 5XFAD control group of the same age. Further analysis revealed that microglia actively phagocytized the amyloid plaques in these both groups. However, the increased numbers and a higher level of microglial cell activation were observed only in the brains of WT 5XFAD mice. Notably, $ST3^{-/-}$ 5XFAD mice did not display significant neuronal loss and they exhibited expression of synaptic markers and cognitive skills comparable with WT and $ST3^{-/-}$ mice without 5XFAD transgenes. Further treatment of 7-month-old WT 5XFAD mice with a sialic acid–binding lectin (*Limax flavus* agglutinin [LFA]) that targets sialic acid on major brain gangliosides resulted in a decreased level of amyloid deposition, inhibited neuroinflammation, and elevated expression of synaptic markers with substantially improved cognitive functions. Thus, our findings demonstrate that targeting brain-specific gangliosides is important for the amelioration of AD pathology and the maintenance of neuronal functions during aging (Fig. S1E).

2. Materials and methods

2.1. Mice

Colonies of B6 (C57BL/6), and st3gal5-deficient ($ST3^{-/-}$) mice (Sotnikov et al., 2013) were maintained at the Laboratory Animal Service Centre of the Chinese University of Hong Kong. $ST3^{-/-}$ mice were backcrossed to the B6 background for at least 12 generations. WT 5XFAD transgenic mice (B6.Cg-Tg(APPSwFlLon, PSEN1*M146L*L286V)6799Vas/Mmjax) were purchased from Jackson Laboratories and maintained at Laboratory Animal Service Centre. For our experiments, we crossed 5XFAD mice with $ST3^{-/-}$ mice to generate $ST3^{-/+}$ 5XFAD mice, which were then crossed with $ST3^{-/-}$ mice to generate $ST3^{-/-}$ 5XFAD mice. Mouse genotyping was performed by standard PCR according to the protocol provided by Jackson Laboratories. The study was performed in accordance with the recommendations of the ARRIVE guidelines (http://www.nc3rs.org.uk/arrive-guidelines). All animal protocols were approved by the Department of Health of the Government of Hong Kong and the Chinese University of Hong Kong Animal Experimentation Ethics Committee. For treatment with LFA, a group of WT 5XFAD mice received i.p. injections of 0.2 mL PBS or 0.2 mL of LFA (20 mg/kg) in PBS per mouse 3 times/week for 5 weeks, after which the Barnes maze cognitive test was performed and the animals were euthanized for histology and real-time RT PCR assays.

2.2. Histochemistry and immunofluorescence

The 7-, 8-, or 12-month-old WT, $ST3^{-/-}$, WT 5XFAD, and $ST3^{-/-}$ 5XFAD mice were perfused with cold PBS, and then 1% paraformaldehyde in PBS. Their brains were dissected and fixed in 1% paraformaldehyde in PBS for 24 hours, then dehydrated in 30% sucrose in PBS for 3–5 days, embedded in Tissue Tek (Sakura) and stored at −80 °C as in our previous studies (Sotnikov et al., 2013). After this, 10-μm-thick frozen sections were prepared using Leica cryotome and stained for Congo red, or FITC-conjugated Thioflavin T (ThT-FITC), or Cresyl violet (all from Sigma) with hematoxyline, and/or with DAPI (Thermo Scientific) according to the standard protocols as we reported earlier (Dukhinova et al., 2018b; Veremeyko et al., 2018). For immunofluorescence, the sections were stained with goat antibodies for Iba1 (BioRad, cat#AHP2024; dilution 1:200) combined with secondary donkey anti-goat antibodies conjugated with AF594 (Abcam, Cat#ab150136; dilution 1:1000), or antibodies for β3-tubulin conjugated with AF488 (Millipore, cat#AB15708A4; dilution 1:1000), or rabbit antibodies for the human APP (BioRad, cat#AHP664; dilution 1:400) that recognizes all forms of full-length hAPP combined with secondary donkey anti-rabbit (Invitrogen, cat#675498; dilution 1:1000) antibodies conjugated with AF546. In addition, 6E10 antibodies that recognize an $A\beta_{1-14}$ portion of APP were purchased from Biolegend (cat#803014; dilution 1:400) and used with secondary antibodies conjugated with AF594 (Thermo Fisher, cat#A-21203; dilution 1:1000). Carl Zeiss Axiophot-2 Microscope Integrated Biological Imaging System and confocal system with an inverted microscope (Olympus FV1000) were used for imaging.

2.3. Western blotting

Western blot analysis was performed according to a standard protocol as previously reported (Ponomarev et al., 2011a; Veremeyko et al., 2018a, b). Antibodies for β-Actin (cat#4967;

dilution 1:1000) were purchased from Cell Signaling. Antibodies for $A\beta_{1-14}$ (clone 6E10) were purchased from Biolegend (cat#803014; dilution 1:1000).

2.4. Analysis of sialic acid content

Concentrations of sialic acid (Neu5Ac) were measured in the brains of 8-month-old WT, $ST3^{-/-}$, WT 5XFAD, and $ST3^{-/-}$ 5XFAD mice using liquid chromatography combined with mass spectrometry (LC/MS) using Agilent 6460 Triple Quadrupole LC/MS System similarly as was described earlier (Dukhinova et al., 2018b; İzzetoğlu et al., 2014; Soya et al., 2017). Briefly, mice were euthanized by swift decapitation, brains were dissected, washed in ice-cold PBS, the homogenized brain tissues were dried, the residues were dissolved in 2M aqueous acetic acid (5 μL per mg of residue), and kept at 80 °C for 3 h to liberate sialic acids. Sialic acids were subjected to further derivatization with 1,2-diamino-4,5-methylenediaoxy-benzene dihydrochloride and determined by LC/MS according to previously published protocol (Soya et al., 2017). Quantitative analysis was performed by using the Agilent MassHunter software. Purified Neu5Ac (Sigma) was used as a standard.

2.5. Ganglioside isolation and analysis

Analysis of ganglioside composition and its quantitation was performed according to previously published protocols (Lopez et al., 2017; Sturgill et al., 2012). Eight-month-old WT, $ST3^{-/-}$, WT 5XFAD, and $ST3^{-/-}$ 5XFAD mice were euthanized by swift decapitation, brains were dissected, washed in ice-cold PBS, split into 2 halves, frozen in dry ice, and kept at −80 °C. After several days, the half brains were weighted (~0.2 g per one-half brain used per each sample), thawed on ice, added 4 volumes of ice-cold water (w/v) and homogenized by a glass-Teflon homogenizer. Methanol was then added to the water phase at the ratio of 8 to 3. The suspension was mixed by vortex, and chloroform was added at the final proportion of chloroform/methanol/water of 4:8:3. The suspension was then vortexed again and centrifuged at 1200 g for 10 minutes at room temperature. The supernatant was collected, the volume was measured with a pipette, and 0.173 volumes of water was added, vortexed, and centrifuged again under the same conditions as aforementioned. The upper phase was collected and evaporated to dryness under a stream of nitrogen gas. The pellet was later dissolved in 400 μL of chloroform/methanol/water (4:8:3) for further analysis. Thin-layer chromatography (TLC) was performed using Silicagel 70 TLC plates 5 × 10 cm (Wako, cat#199-17874). The 3 μL of each sample or standards was applied on the TLC plate. As a developing solvent system, we used chloroform/methanol/0.25% aqueous potassium chloride (60:35:8) solution. Gangliosides were visualized by spraying resorcinol reagent at 125 °C for 20 minutes. Purified GM1, GD3 (both from Sigma), and GQ1b (Calbiochem) were used as standards.

2.6. Flow cytometry and cell sorting

The mice were perfused with PBS, and the brains were dissected, homogenized, and mononuclear cells were isolated using a 40%/70% Percoll gradient as described previously (Dukhinova et al., 2018a; Ponomarev et al., 2011a; Veremeyko et al., 2012). Brain mononuclear cells were stained with anti-CD11b-AF488 (BD Biosciences), anti-Ly6C-PE (BD Biosciences), anti-CD45-APC-Cy7 (Biolegend), anti-CD86-AF647 (Biolegend) and anti-MHC class II-PerCP-Cy5.5 (Biolegend) antibodies and analyzed by 5-color flow cytometry as previously described (Dukhinova et al., 2018a; Ponomarev et al., 2000, 2011a; Sotnikov et al., 2013; Starossom et al., 2015; Veremeyko et al., 2012, 2018b). Samples were analyzed using a BD LSRFortessa Flow Cytometer (BD Biosciences).

For the cell sorting, mononuclear cells were isolated from brains of 8-month-old WT, $ST3^{-/-}$, WT 5XFAD, and $ST3^{-/-}$ 5XFAD mice, stained for CD11b, and $CD11b^{+}$ gated cells were sorted into Eppendorf tubes with 700 μL of QIAzol Lysis Reagent (Qiagen) using BD Aria Fusion Cell sorter (BD Biosciences) for subsequent RNA isolation.

2.7. RNA isolation and real-time RT PCR

For RNA isolation from brain tissue and cultured cells, the samples were homogenized and lysed using QIAzol Lysis Reagent (Qiagen) as described previously (Pavlov et al., 2019; Ponomarev et al., 2011a, b; Veremeyko et al., 2012). RNA purification with DNase digestion was performed using a miRNeasy Mini Kit from Qiagen. Real-time RT PCR was performed using ABI ViiA 7 and ABI QuantStudio 7 (QS7) Flex Systems. For analysis of mRNA expression, the following primers were used: PSD95 (forward 5′-TCTGTGCGAGAGGTAGCAGA-3′; reverse 5′-AAGCACTCCGTGAACTCCTG-3′), Syn1α, (forward 5′-CCGCCAGCTGCCTTC-3′, reverse 5′-TGCAGCCCAATGACCAAA-3′), IL-1β (forward 5′-CTTCCAGGATGAGGACATGAGCAC-3′, reverse 5′-TCATCATCCCATGAGTCACAGAGG-3′), TNF (forward 5′-AGCCGATGGGTTGTACCTTG-3′, reverse 5′-GTGGGTGAGGAGCACGTAGTC-3′). Relative expression was calculated using the ΔC_T method and normalized to the GAPDH housekeeping gene (forward primer, 5′-ATGACCACAGTCCATGCCATC-3′; reverse primer, 5′-GAGCTTCCCGTTCAGCTCTG-3′), and then the relative level of expression was calculated in comparison with control samples.

2.8. Barnes maze test

For the Barnes maze cognitive test, we used a white circular platform (92 cm in diameter) with 20 equally spaced holes (5 cm diameter; 7.5 cm between holes) according to a previously elaborated protocol described in the following shared online resource: https://www.nature.com/protocolexchange/protocols/349#.
Groups of 3–5 mice were trained to locate a hole through which they could escape from the apparatus to an escape box during daily training sessions for 4 days. Latency to escape was scored manually on days 1–4. On day 5, a final trial was performed, in which the animals could not escape the apparatus and their latency time to finding the closed target hole and time spent in the area of the closed target hole was evaluated offline using the Noldus Ethovision XT 11 software. Latency time was used as a measure of test performance in the final trial.

2.9. Statistical analysis

The results are presented as bar graphs showing mean ± S. E., or as whisker plots with median and 10%/90% percentiles, and the mean value indicated by a "+" symbol as indicated in figure legends. Unpaired Student's t-tests were used to determine significance between 2 experimental groups. p values of less than 0.05 were considered significant. SigmaPlot and GraphPad Prizm software were used to create the charts and perform statistical analysis.

3. Results

3.1. $ST3^{-/-}$ 5XFAD 8- and 12-month-old mice have a low amyloid plaque burden and do not exhibit signs of brain atrophy

It is known from the literature that WT 5XFAD mice start to exhibit widespread amyloid depositions in the cortex and decline in cognitive function at 4–6 months of age, whereas neuronal loss and a decrease in the expression of synaptic markers PSD95 and Syn-1

has been observed at 9–12 months (Oakley et al., 2006). Based on these data, we compared amyloid depositions in WT and ST3$^{-/-}$ 5XFAD mice at 8 and 12 months of age when all manifestations of AD pathology were observed in the WT 5XFAD mice. We found that the density of amyloid plaques was 2-fold and 3-fold lower in the cortex of ST3$^{-/-}$ 5XFAD mice when compared with WT 5XFAD mice of 8 and 12 months of age, respectively (Fig. 1A and B). Although amyloid plaques were still detected in very small numbers in ST3$^{-/-}$ 5XFAD mice, these plaques were smaller and/or less dense as determined by Congo red staining (Fig. 1A). At 8 months of age, the WT 5XFAD mice already exhibited clear signs of brain atrophy, which was manifested by a decrease in average brain weight when compared with age-matched WT control mice (Fig. 1C). Strikingly, 8-month-old ST3$^{-/-}$ 5XFAD mice did not exhibit signs of brain atrophy and had average brain weights comparable with age-matched WT or ST3 control groups without FAD transgenes (Fig. 1C). These data reveal ameliorated AD pathology in ganglioside-deficient 5XFAD mice.

3.2. ST3$^{-/-}$ 5XFAD mice have a low level of β-amyloid and its fragments

Next, we compared the level of amyloid depositions in 8-month-old WT versus st3gal5-deficient 5XFAD mice by using a combination of immunofluorescent stinging and western blot analysis and 6E10 antibody that recognizes Aβ$_{1\text{-}14}$. We found that WT 5XFAD mice have a substantial level of Aβ accumulation in hippocampal area, which was very low in ST3$^{-/-}$ 5XFAD mice as well as WT and ST3$^{-/-}$ mice without 5XFAD transgene (Fig. 2A and B). Western blot analysis also demonstrated the presence of a substantial level of 4 kDa monomers for Aβ in WT 5XFAD mice, which was 11-fold lower in ST3$^{-/-}$ 5XFAD animals (Fig. 2C and D). This data further

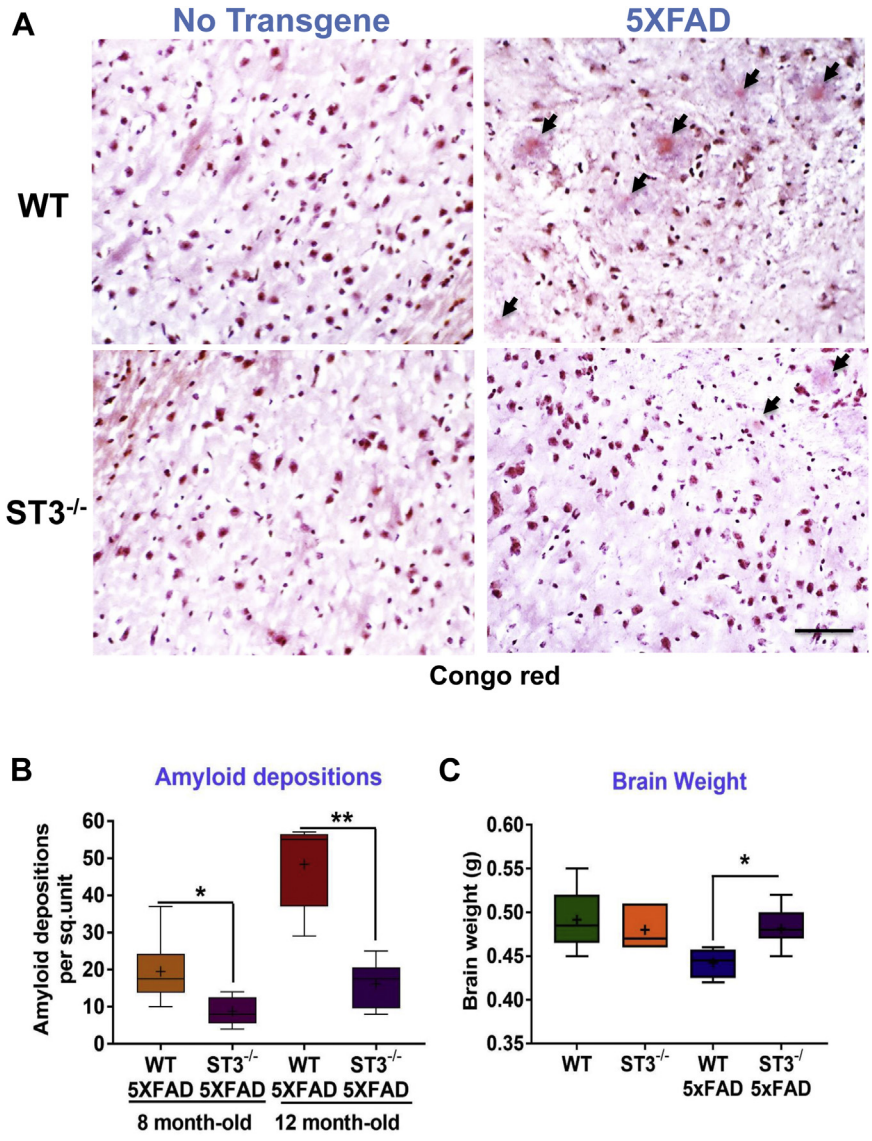

Fig. 1. Analysis of amyloid plaque burden in the brain cortex and the brain weight of aged WT, ST3$^{-/-}$, WT 5XFAD, and ST3$^{-/-}$ 5XFAD mice. (A) Brain histology sections of 8-month-old control WT, ST3$^{-/-}$, WT 5XFAD, and ST3$^{-/-}$ 5XFAD mice were stained with Congo red and counterstained with hematoxylin as described in Materials and Methods. Amyloid depositions are indicated by arrows. Scale bar: 100 μm (B) Quantitative analysis of plaque numbers in the brain cortical area of 8- and 12-month-old WT 5XFAD and age-matched ST3$^{-/-}$ 5XFAD mice. (C) Quantitative analysis of wet brain weight of 8-month-old WT, ST3$^{-/-}$, WT 5XFAD, and ST3$^{-/-}$ 5XFAD mice. The weight of each brain was measured on a laboratory scale after whole-body perfusion with PBS and subsequent dissection. Whisker plots with median and 10%/90% percentiles of 5–8 individual animals are shown in B and C (*, $p < 0.05$; **, $p < 0.01$). Mean values are indicated by "+" symbols. (For interpretation of the references to color in this figure legend, the reader is referred to the Web version of this article.)

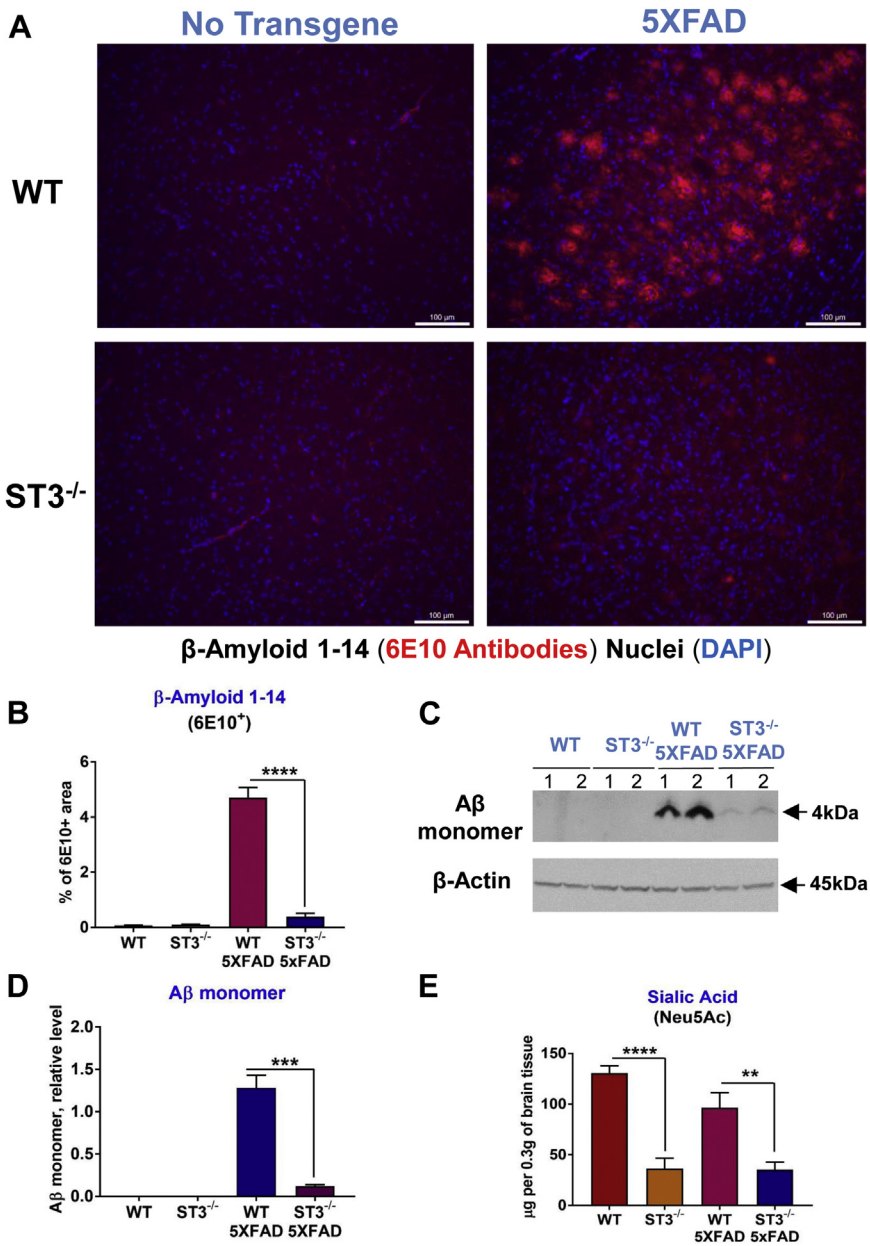

Fig. 2. Analysis of amyloid depositions and sialic acid content in the brains of WT, ST3$^{-/-}$, WT 5XFAD, and ST3$^{-/-}$ 5XFAD mice. (A, B) Brain histology sections of 8-month-old WT, ST3$^{-/-}$, WT 5XFAD, and ST3$^{-/-}$ 5XFAD mice were prepared and stained for amyloid depositions with 6E10 antibodies for A$\beta_{1\text{-}14}$ (red) and nuclear marker DAPI (blue) as described in Materials and Methods. Scale bar: 100 μm. A representative image is shown in (A); quantitative analysis of 6E10^{+} covered area is shown in (B). (C, D) Western blot analysis for Aβ monomer content in the brains of 8-month-old WT, ST3$^{-/-}$, WT 5XFAD, and ST3$^{-/-}$ 5XFAD mice. For detection of 4 kDa Aβ monomer, 6E10 antibody was used and staining for β-Actin was used as a loading control as described in Materials and Methods. Representative images are shown in C for 2 individual mice (labeled as 1 and 2). Quantitative analysis is shown in D. (E) Analysis of sialic acid content in the brains of 8-month-old WT, ST3$^{-/-}$, WT 5XFAD, and ST3$^{-/-}$5XFAD mice. Quantitative analysis of sialic acid (Neu5Ac) was performed using LC/MS methods as described in Materials and Methods. In B, D, and E, mean ± S.D. is shown (n = 5 mice; **, $p < 0.01$; ***, $p < 0.001$; ****, $p < 0.0001$). (For interpretation of the references to color in this figure legend, the reader is referred to the Web version of this article.)

demonstrated a significant reduction in amyloid depositions in ST3$^{-/-}$ 5XFAD mice.

3.3. ST3$^{-/-}$ 5XFAD mice have a reduced level of sialic acid in the brain

We compared the composition of gangliosides in the brains of 8-month-old WT, ST3$^{-/-}$, WT 5XFAD, and ST3$^{-/-}$ 5XFAD mice. As it was reported earlier (Yoshikawa et al., 2009), ST3$^{-/-}$ mice do not have a-, b-, and c-series gangliosides, but have elevated levels of GM1b and GD1α that were visualized as 2 major bands for ST3$^{-/-}$ mice on TLC (Fig. S2A, WT vs. ST3$^{-/-}$). WT 5XFAD and ST3$^{-/-}$ 5XFAD had ganglioside compositions comparable with WT and ST3$^{-/-}$ mice without 5XFAD transgenes, respectively (Fig. S2A, WT 5XFAD, and ST3$^{-/-}$ 5XFAD). Quantitative analysis indicated 2-fold decrease in ganglioside content in ST3$^{-/-}$ mice (with or without 5XFAD transgene) when compared with WT mice (with or without 5XFAD transgene, respectively) (Fig. S2B). These data indicated that ST3$^{-/-}$ 5XFAD mice had a lower level of gangliosides and sialic acid in general, which was further

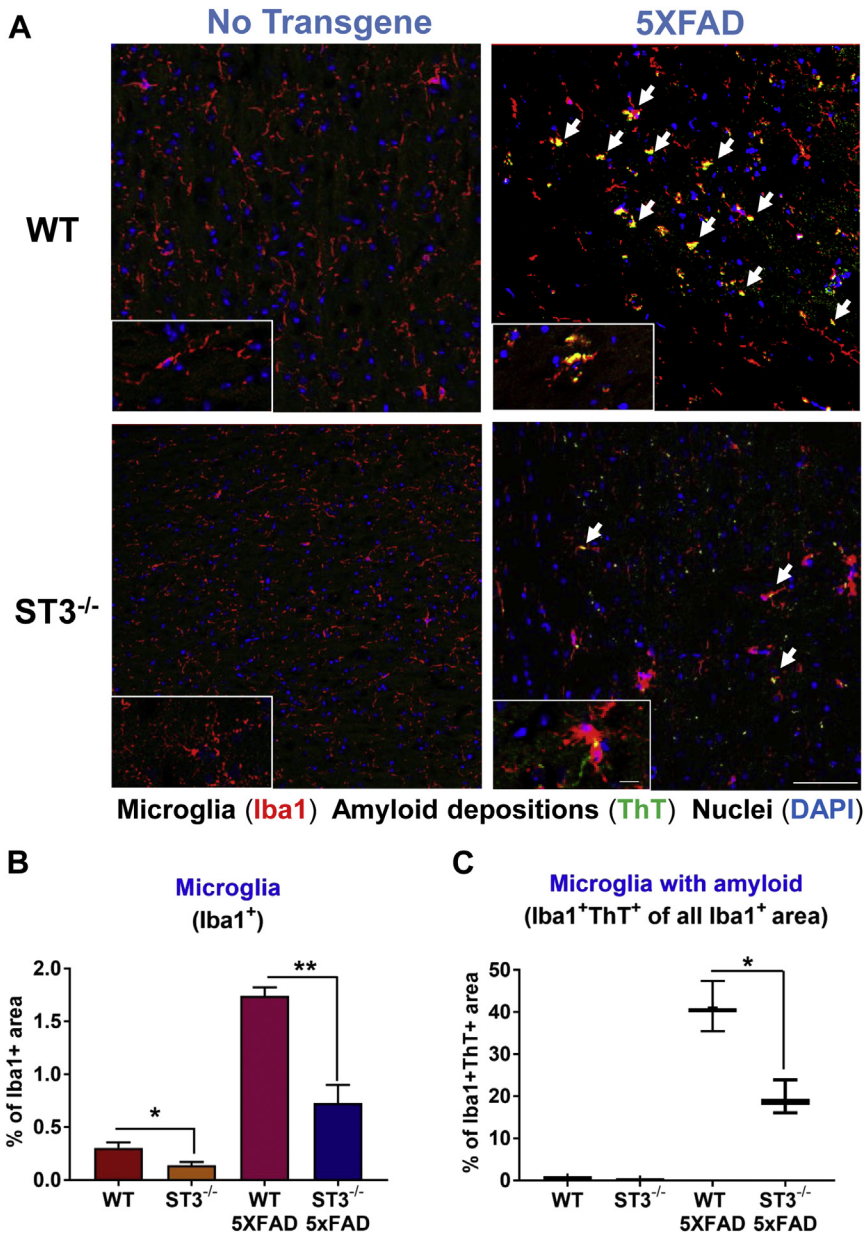

Fig. 3. Comparison of the level of microglia activation in areas of amyloid depositions in the brain cortex of WT 5XFAD and ST3$^{-/-}$ 5XFAD mice. (A) Brain histology sections of 8-month-old WT, ST3$^{-/-}$, WT 5XFAD, and ST3$^{-/-}$ 5XFAD mice were prepared and stained for amyloid depositions with ThT-FITC (green), microglial cell marker Iba1 (red), and nuclear marker DAPI (blue) as described *in* Materials and Methods. Sites of colocalization of amyloid depositions and microglia (yellow) are marked with arrows. Scale bars: 100 μm (lower magnification) and 10 μm (higher magnification). (B) Quantitative analysis of Iba1^{+} microglial cell covered area in brain cortical areas where amyloid depositions were evident for WT 5XFAD and ST3$^{-/-}$ 5XFAD mice. (C) Quantitative analysis of the percentage of Iba1^{+}microglia colocalized with ThT^{+} amyloid depositions in the brain cortical areas where amyloid depositions were evident for WT 5XFAD and ST3$^{-/-}$ 5XFAD mice. In B and C, analysis of sections from 3–4 animals with a total number of 15–20 section images is shown. Whisker plots with median and 10%/90% percentiles of 15–20 images are shown (*, $p < 0.05$; **, $p < 0.01$). Mean values are indicated by "+" symbols. (For interpretation of the references to color in this figure legend, the reader is referred to the Web version of this article.)

confirmed by mass spectrometry analysis of sialic acid in the brains of WT, ST3$^{-/-}$, WT 5XFAD, and ST3$^{-/-}$ 5XFAD mice. This analysis demonstrated a 3- to 4-fold reduction in the level of sialic acid in the brain of st3gal5-deficient animals (Fig. 2E). It was a slight reduction in sialic acid content in WT 5XFAD mice when compared with WT animals (Fig. 2E), which could be explained by the on-going process of neurodegeneration and decrease in brain weight (Fig. 1C), as well as decreased level of gangliosides (Fig. S2B; WT vs. WT 5XFAD). Thus, these data demonstrated the reduction of the number of gangliosides and sialic acid in ST3$^{-/-}$ 5XFAD mice.

3.4. ST3$^{-/-}$ 5XFAD mice do not demonstrate substantial morphological changes associated with activation of microglia, but these cells were still capable of amyloid phagocytosis

It is known that during AD, and in mouse models of the disease, microglia become activated and there is AD-associated neuro-inflammation (Hansen et al., 2018; Heneka et al., 2015). Therefore, we evaluated morphological changes associated with microglia activation and colocalization with amyloid deposits in the cortex of 8-month-old WT 5XFAD and ST3$^{-/-}$ 5XFAD mice (Fig. 3A; *5XFAD*). Age-matched WT and ST3$^{-/-}$ mice without the FAD transgene were used as controls

(Fig. 3A; no transgene). We found that in the CNS of WT 5XFAD mice Iba1-positive microglial cells showed clear morphological signs of activation when compared with WT controls, as determined by the increases in cell size and cell number (Fig. 3A and B; WT 5XFAD). By contrast, ST3$^{-/-}$ 5XFAD mice showed only mild signs of microglia activation when compared with ST3$^{-/-}$ controls as determined by the increases in cell size and cell number (Fig. 3A and B; ST3$^{-/-}$ 5XFAD). In addition, the background level of microglia activation was lower in ST3$^{-/-}$ mice than in WT mice without the FAD transgene (Fig. 3B; WT and ST3$^{-/-}$). However, the microglia in ST3$^{-/-}$ 5XFAD mice were still co-colorized with ThT-positive amyloid depositions, indicating ongoing amyloid phagocytosis (Fig. 3A; ST3$^{-/-}$ 5XFAD). In the WT 5XFAD mice, ~40% of microglia were phagocytizing ThT-positive amyloid depositions, whereas 20% of microglia were phagocytizing amyloid depositions in the ST3$^{-/-}$ 5XFAD mice (Fig. 3C). These data indicate that microglia were less activated in ST3$^{-/-}$ 5XFAD, but still capable of phagocytizing amyloid depositions.

3.5. ST3$^{-/-}$ 5XFAD mice have low levels of monocyte and lymphocyte infiltration in the CNS

During neuroinflammation, other Iba1-positive cells, such as peripheral monocytes/macrophages, may be present in the CNS of 8-month-old 5XFAD mice (Ponomarev et al., 2005). We, therefore, evaluated the extent of infiltration of peripheral monocytes/macrophages and lymphocytes in the WT, ST3$^{-/-}$, WT 5XFAD, and ST3$^{-/-}$ 5XFAD mice using multicolor flow cytometry to analyze the expression of CD11b, Ly6C, and CD45. According to previous studies, peripheral monocytes can be determined in the CNS as CD11b^{+}Ly6C^{+} cells, whereas lymphocytes can be determined as CD11b^{+}CD45^{hi} cells, and microglia are represented by CD11b^{+}CD45$^{low/int}$Ly6C^{-} cells (Dukhinova et al., 2018b; Mayo et al., 2014; Ponomarev et al., 2005). Although Ly6C could clearly distinguish peripheral monocytes in acute models such as traumatic brain injury (Dukhinova et al., 2018b), Ly6C-negative peripheral myeloid cells could be present in the CNS in a chronic model of AD. We found that in the WT and ST3$^{-/-}$ mice, peripheral monocytes constituted 1%–2% of all brain mononuclear cells, whereas in the WT 5XFAD mice, their number increased to an average of 4% but remained close to 2% in the ST3$^{-/-}$ 5XFAD mice (Fig. 4A and C). At the same time, the percentage of CD11b^{+}Ly6C^{-} microglia was increased in ST3$^{-/-}$ 5XFAD (92%) when compared with WT 5XFAD animals (86%). Lymphocytes were present in the WT and ST3$^{-/-}$ mice at a level of 2%–3% of all brain mononuclear cells, while their level was increased to an average of 7% in the 5XFAD mice and to 4% in ST3$^{-/-}$ 5XFAD mice (Fig. 4B and D). Thus we found that the levels of peripheral monocytes and lymphocytes were low in the WT, ST3$^{-/-}$, WT FAD, and ST3$^{-/-}$ FAD mice; and the levels of peripheral monocytes and lymphocytes were reduced ~2-fold in the CNS of ST3$^{-/-}$ 5XFAD mice when compared with WT 5XFAD animals.

3.6. Microglia from ST3$^{-/-}$ 5XFAD mice have a low level of expression of activation markers MHC class II and CD86

We further investigated the extent of activation of microglia. To exclude peripheral monocytes/macrophages, we analyzed CD11b^{+}CD45$^{low/int}$Ly6C^{-} gated cells for the expression of known activation markers for microglia MHC class II (Fig. 5A and C) and CD86 (Fig. 5B and D). The gating strategy is shown in Fig. S3. As we motioned earlier, this strategy allows identifying most CNS-resident microglial cells; however, Ly6C-negative peripheral cells could be also present in this population. We found that both activation markers were upregulated in the WT 5XFAD mice when compared with the WT controls, whereas in the ST3$^{-/-}$ 5XFAD mice, the expression of MHC class II and CD86 decreased ~2-fold to levels comparable with WT or ST3$^{-/-}$ controls (Fig. 5A–D). Thus, the levels of expression of MHC class II and CD86 on microglia were significantly reduced in the CNS of ST3$^{-/-}$ 5XFAD mice.

3.7. ST3$^{-/-}$ 5XFAD mice do not exhibit neuronal loss and have very low levels of amyloid deposition in the brain

We found that the WT 5XFAD mice exhibited signs of brain atrophy as determined by a decrease in brain weight (Fig. 1C) (Esiri, 2007). Another sign of atrophy and cognitive decline is an increase in the volume of the perivascular space (Favaretto et al., 2017; Zhang et al., 2016). Using Cresyl violet staining, we found an increased volume of perivascular space in the cortex of the WT 5XFAD mice compared with the WT and ST3$^{-/-}$ controls. The increase in the volume of the perivascular space was much less evident in the ST3$^{-/-}$ 5XFAD mice (Fig. 6A and C). To further evaluate neuronal loss in the area of amyloid depositions accumulation, we stained for the neuronal marker β3-tubulin and human full-length APP. We found that neuronal loss was evident in hAPP-positive areas of the WT 5XFAD mice but not the ST3$^{-/-}$ 5XFAD mice (Fig. 6B and D). We confirmed that hAPP load was significantly lower in the areas of amyloid deposition in the ST3$^{-/-}$ 5XFAD mice when compared with WT 5XFAD mice (Fig. 6B and E). These findings demonstrate that ST3$^{-/-}$ mice do not exhibit a substantial neuronal loss in the areas of amyloid deposition.

3.8. ST3$^{-/-}$ 5XFAD mice do not exhibit downregulated proinflammatory cytokines IL-1β and TNF but have upregulated synaptic markers PSD95 and Syn-1

In addition to assessing the infiltration of peripheral leukocytes, microglia activation, and neuronal loss, we examined the expression of 2 main proinflammatory cytokines, TNF and IL-1β, and 2 main synaptic markers, PSD95 and Syn1α. As expected, both TNF and IL-1β were upregulated in the WT 5XFAD mice when compared with the control WT group (Boza-Serrano et al., 2018; Landel et al., 2014). However, the expression of *TNF* in the ST3$^{-/-}$ 5XFAD mice was at the same level as in the WT 5XFAD mice, whereas expression of *IL-1β* was elevated ~2-fold (Fig. 7A and B). These results were unexpected because microglia in st3gal5-deficient animals had a lower level of activation and it was less infiltrating CD11b^{+}LyC6^{+} monocytes (Figs. 4 and 5). To address this conundrum, we looked at the level of IL-1β expression in CNS CD11b^{+} cells in WT, ST3, WT 5XFAD, and ST3$^{-/-}$ 5XFAD mice. We found that CD11b cells in ST3$^{-/-}$ 5XFAD mice had a comparable level of IL-1β expression (Fig. S4). Based on these finding, we hypothesized that astrocytes produce more IL-1β in ST3$^{-/-}$ 5XFAD mice. In support of our hypothesis, we have previously found that ST3$^{-/-}$ mice higher level of astrogliosis after brain injury indicating a higher level of astroglial activation in these mice when compared with WT animals (Dukhinova et al., 2018b).

Expression of *PSD95* and *Syn1α* was reported to be decreased in 9-month-old WT 5XFAD mice (Oakley et al., 2006). We confirmed this for 8-month-old WT 5XFAD mice, in which both markers were decreased when compared with the WT controls (Fig. 7C and D; WT and WT 5XFAD). The expressions of both markers were elevated in the ST3$^{-/-}$ mice when compared with the WT mice (Fig. 7C and D; *WT* and *ST3*$^{-/-}$), and stayed high in the ST3$^{-/-}$ 5XFAD mice (Fig. 7C and D; ST3$^{-/-}$ 5XFAD). These data demonstrate that in contrast to the WT 5XFAD mice, the level of synaptic markers was not downregulated in the ST3$^{-/-}$ 5XFAD mice.

3.9. The cognitive performance of ST3$^{-/-}$ 5XFAD mice is comparable with that of WT controls

As the ST3$^{-/-}$ 5XFAD mice had a low level of amyloid depositions, did not demonstrate significant neuronal loss, and had

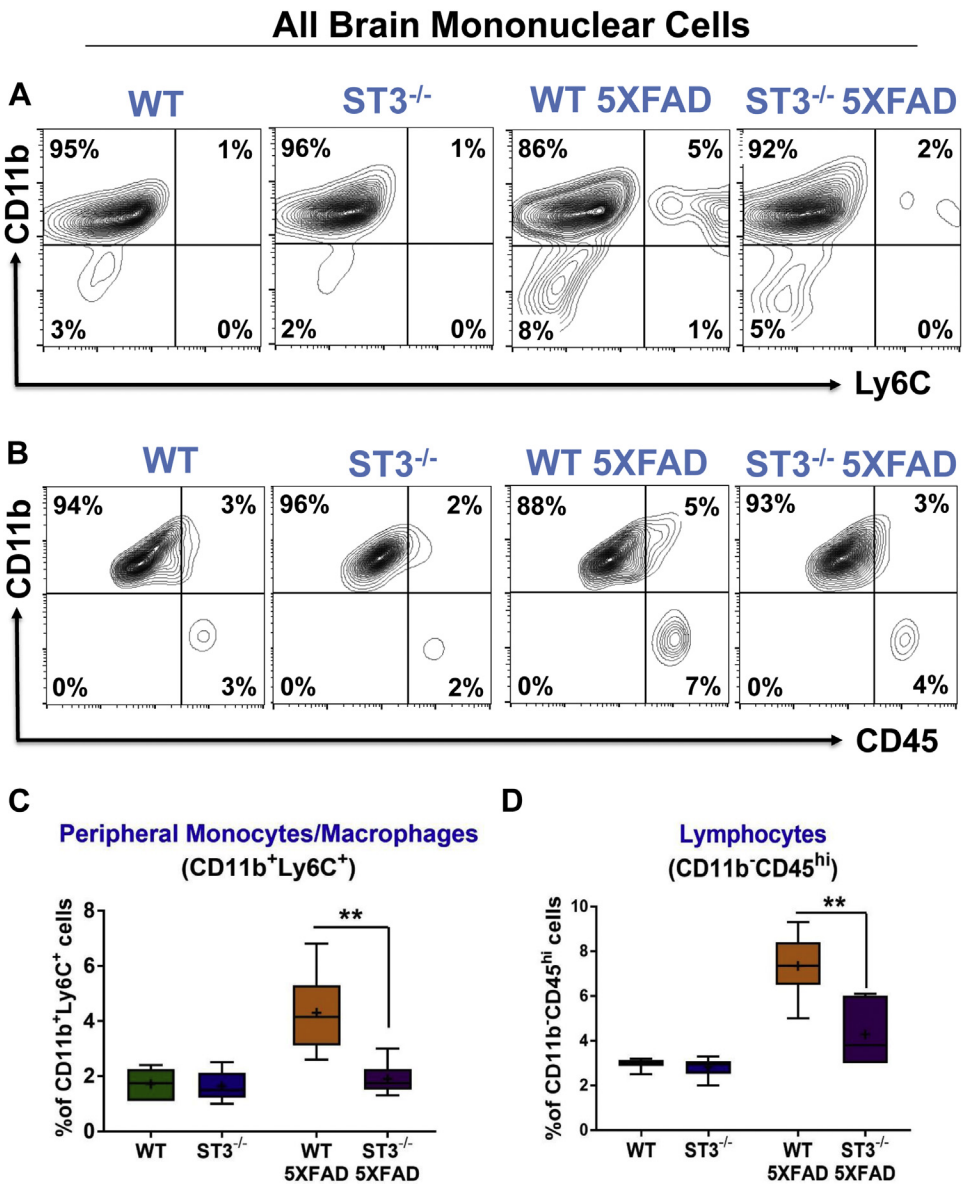

Fig. 4. Comparison of extent of infiltration of peripheral monocytes and lymphocytes in the brain cortex of WT 5XFAD and ST3$^{-/-}$ 5XFAD mice. (A, B) Analysis of microglia activation and macrophage infiltration in the brains of 8-month-old WT, ST3$^{-/-}$, WT 5XFAD, and ST3$^{-/-}$ 5XFAD mice. Mononuclear cells were isolated from the brain and analyzed for expression of CD11b, Ly6C, and CD45 by flow cytometry. (A) Representative contour-plots for expression of Ly6C (x-axes) and CD11b (y-axes) are shown. The quadrants distinguish populations of CD11b^{+}Ly6C^{-} (microglia), CD11b^{+}Ly6C^{+} (peripheral monocytes/macrophages), and CD11b^{-}Ly6C^{-} and CD11b^{-}Ly6C^{+} cells (both are lymphocytes). The percentage of each population is shown in the corner of each quadrant. (B) Representative contour-plots for expression of CD45 (x-axes) and CD11b (y-axes) are shown. The quadrants distinguish populations of CD11b^{+}CD45$^{low/int}$ (microglia), CD11b^{+}CD45^{hi} (peripheral monocytes/macrophages), CD11b^{-}CD45^{-} (contaminating astroglial cells), and CD11b^{-}CD45^{hi} cells (lymphocytes). The percentage of each population is shown in the corner of each quadrant. In C and D, quantitative analysis of percentages of CD11b^{+}Ly6C^{+} peripheral monocytes/macrophages (C) and CD11b^{-}CD45^{hi} lymphocytes (D) is shown. The data are representative of 4 experiments with a total number of 12–15 mice. Whisker plots with median and 10%/90% percentiles of 12 (C) or 15 (D) individual animals are shown (**, $p < 0.01$; n = 12–15 mice). Mean values are indicated by "+" symbols.

normal levels of synaptic markers, we expected that these mice would have intact cognitive abilities. To test this, we used a Barnes maze test that measures spatial learning and memory (Rosenfeld and Ferguson, 2014). Interestingly, on day 1 of training, only the WT mice had good performance, whereas the ST3$^{-/-}$ mice showed the same delayed learning process as the WT 5XFAD and ST3$^{-/-}$ 5XFAD mice (Fig. 7E; Day 1). On day 2 of training, the st3gal5-deficient mice showed the same performance as the WT mice, whereas the ST3$^{-/-}$ 5XFAD mice still had a similar performance to the WT 5XFAD mice (Fig. 7E; Day 2). On day 3, the performance of the ST3$^{-/-}$ 5XFAD, but not the WT 5XFAD mice, was significantly improved and reached a level close to that of the WT mice by day 4 (Fig. 7E; *Day 3* and *Day 4*). In the final trial on day 5, the performance of the ST3$^{-/-}$ 5XFAD mice was comparable with that of the WT and ST3$^{-/-}$ controls (Fig. 7F). These results demonstrate that the ST3$^{-/-}$ 5XFAD mice had spatial and memory functions comparable with the WT controls.

3.10. Treatment of WT 5XFAD mice with sialic acid–specific lectin results in improved performance on the cognitive test, decreased amyloid depositions, normalized expression of synaptic markers, and reduced neuroinflammation

As the absence of major brain gangliosides in the ST3$^{-/-}$ mice was associated with significantly improved AD pathology, we hypothesized that targeting the surface of gangliosides may be

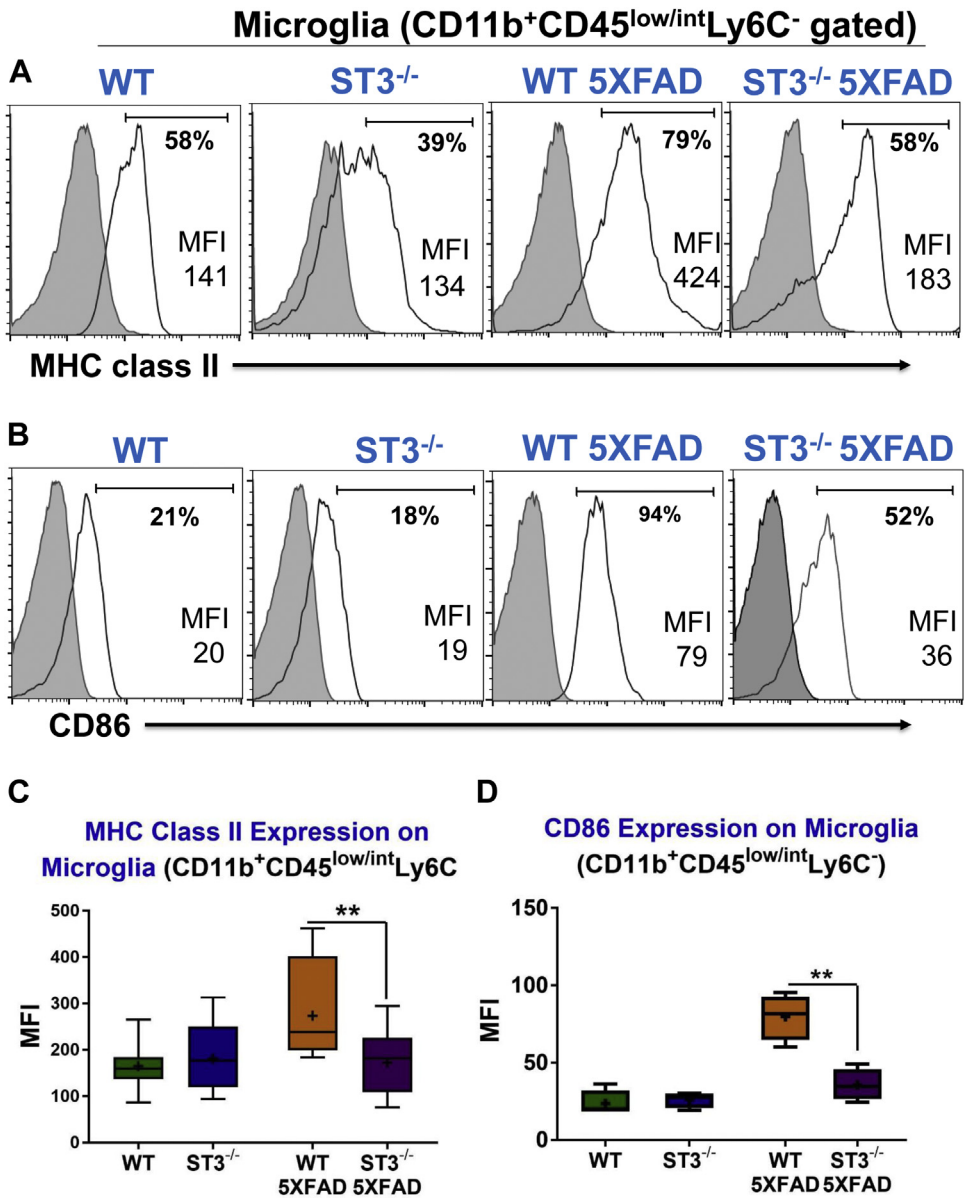

Fig. 5. Comparison of the expression levels of microglia activation markers MHC class II and CD86 in the brain cortex of WT 5XFAD and ST3$^{-/-}$ 5XFAD mice. Analysis of microglia activation in the brain of 8-month-old WT, ST3$^{-/-}$, WT 5XFAD, and ST3$^{-/-}$ 5XFAD mice. Mononuclear cells were isolated from the brain and analyzed for expression of CD11b, Ly6C, CD45, MHC class II, and CD86 by five-color flow cytometry as described in Materials and Methods. Brain resident microglial cells were gated as CD11b^{+}CD45$^{low/int}$Ly6C^{-} and as shown in Fig. S3 and analyzed for the expression of activation markers MHC class II and CD86. (A, B) Representative histograms for expressions of MHC class II (A) and CD86 (B) on CD11b^{+}CD45$^{low/int}$Ly6C^{-} gated microglia are shown. The solid lines represent staining for MHC class II or CD86, and the dotted lines represent staining for isotype-matched controls. Percentages of positive cells are shown below linear gates and mean fluorescent intensity (MFI) values are shown in the bottom left corner of each histogram. In C–D, the quantitative analysis of MFI levels for MHC class II (C) and CD86 (D) is shown. Whisker plots with median and 10%/90% percentiles of 12 (C) and 5 (D) individual animals are shown (**, $p < 0.01$). Mean values are indicated by "+" symbols. (For interpretation of the references to color in this figure legend, the reader is referred to the Web version of this article.)

beneficial for AD. It is known that sialic acid is exposed to the outer surface of glycolipids and glycoproteins (Varki, 2008). Moreover, sialic acid has been shown to be critical for the binding of amyloid peptides to brain gangliosides (Ariga et al., 2001). In the CNS, ~75% of total sialic acid mass belongs to gangliosides (Schnaar et al., 2014). Therefore, there is the possibility of blocking sialylated acid on the surface of gangliosides using sialic acid–specific lectins. LFA lectin specifically binds to sialic acid and has a low level of toxicity (Knibbs et al., 1993; Sotnikov et al., 2013). We started treatment of 6-month-old WT 5XFAD, which are known to have distinct symptoms of AD as determined by definitive cognitive problems by the age of 6 months (Oakley et al., 2006). We treated 6-month-old WT 5XFAD mice with i.p. injection of LFA 3 times a week for 5 weeks. We then administered the cognitive test, to compare the functional results with pathology analysis of brain tissues (Fig. 8A). We found significantly improved performance in the LFA- versus PBS-treated WT 5XFAD mice on days 3 and 4 of training (Fig. 8B) and in the final trial (Fig. 8C). When we analyzed the cortical areas of these mice, we found a significant decrease in amyloid plaque burden in the LFA-treated WT 5XFAD mice as determined by histology (Fig. 8D and E) and western blot analysis of Aβ monomers (Fig. 8F and G). LFA treatment significantly upregulated expression of *PSD95* and *Syn1α* in WT 5XFAD mice to levels exceeding those of the WT controls and similar to those of the ST3$^{-/-}$ and ST3$^{-/-}$ FAD mice (Fig. 9A and B). Treatment of the WT 5XFAD mice with LFA decreased expression of *TNF* 1.5-fold and expression of *IL-1β* 3-fold

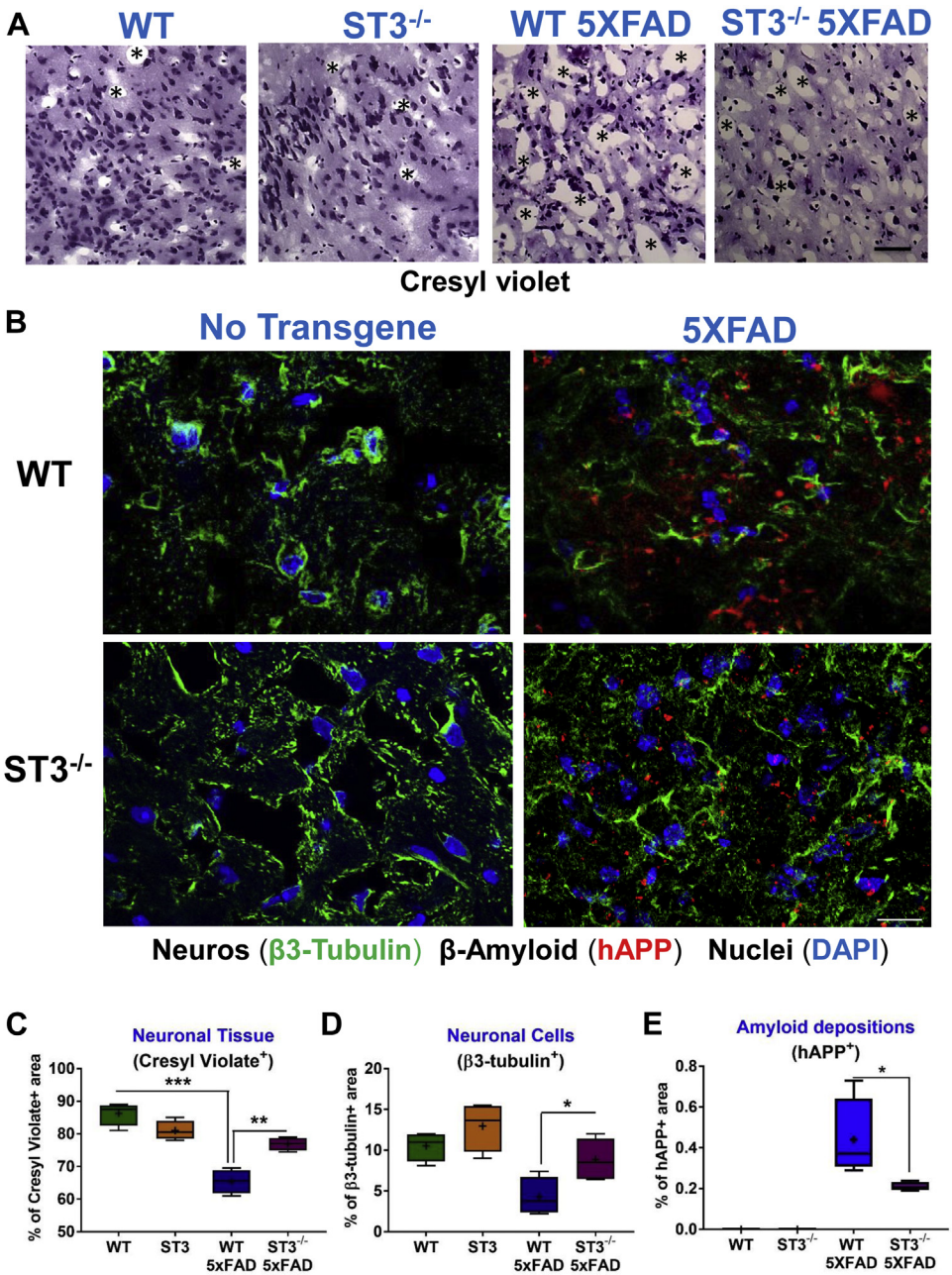

Fig. 6. Analysis of extent of amyloid-related neuronal damage and atrophy in the brain cortex of WT 5XFAD and ST3$^{-/-}$ 5XFAD mice. (A) Brains of 8-month-old WT, ST3$^{-/-}$, 5XFAD, and ST3$^{-/-}$ 5XFAD were collected for histology analysis and stained with Cresyl violet dye as described in Materials and Methods. Representative images are shown. The centers of representative perivascular areas are indicated by "*" symbols. Scale bar: 100 μm . (B) Brain histology sections of 8-month-old WT, ST3$^{-/-}$, 5XFAD, and ST3$^{-/-}$ 5XFAD mice were stained for neuronal marker (β3-tubulin; green), human APP (hAPP; red), and nuclei (DAPI; blue). Scale bar: 25 μm. In C–E, the quantification of Cresyl violet–covered (neuronal tissue; C), the neuronal cell-covered (β3-tubulin^{+}; D) and full-length amyloid-covered (hAPP^{+}; E) areas in the brain sections of WT, ST3$^{-/-}$, 5XFAD, and ST3$^{-/-}$ 5XFAD mice is shown. Whisker plots with median and 10%/90% percentiles of 4–5 individual animals are shown (n = 4-5; *, $p < 0.05$; **, $p < 0.01$; ***, $p < 0.001$). Mean values are indicated by "+" symbols. (For interpretation of the references to color in this figure legend, the reader is referred to the Web version of this article.)

(Fig. 9C and D). Similarly, LFA treatment decreased activation of microglia (Fig. 9E and F) and the percentage of microglia associated with amyloid depositions (Fig. 9E and G). These findings demonstrate that treatment of WT 5XFAD mice with LFA significantly ameliorated AD pathology and neuroinflammation.

4. Discussion

In this study, we investigated the role of brain gangliosides in AD pathology in a 5XFAD mouse model with overexpression of human mutated APP and PS1 genes. We found that 5XFAD mice that lack all major brain gangliosides had significantly reduced levels of amyloid depositions and decreased levels of both neurodegeneration and CNS inflammation. Moreover, treating the WT 5XFAD mice with a sialic acid–specific lectin for one month resulted in significant improvement of AD pathology as determined by decreased levels of amyloid depositions and neuroinflammation and upregulated synaptic markers and significantly improved cognitive abilities. Notably, LFA treatment resulted in a similar phenotype to that observed in ST3$^{-/-}$ 5XFAD mice (Fig. S1E).

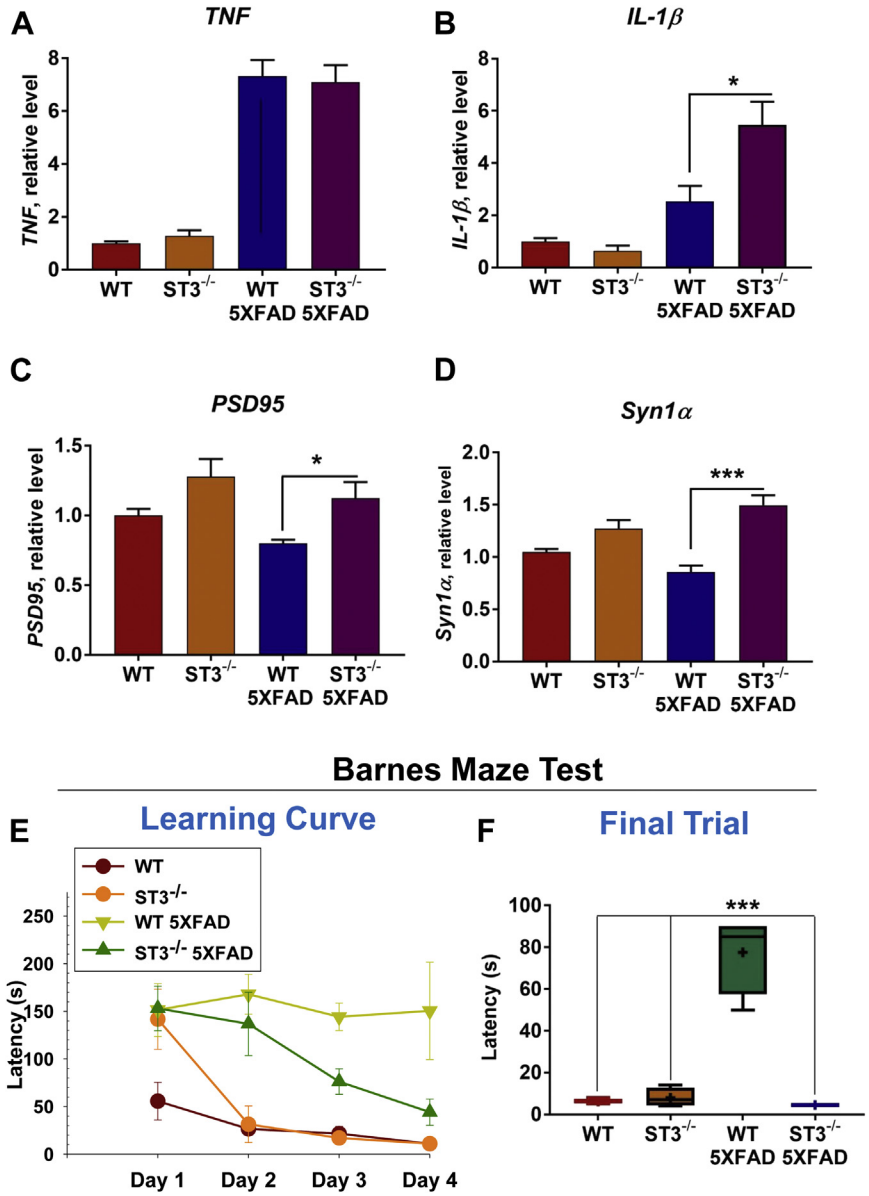

Fig. 7. Comparison of the expression levels of proinflammatory cytokines IL-1β and TNF and synaptic markers PSD95 and Syn-1 in the brain cortex of WT 5XFAD and ST3$^{-/-}$ 5XFAD mice. (A–D) Analysis of mRNA expression levels of proinflammatory cytokines TNF (A) and IL-1β (B), and neuronal synaptic markers PSD95 (C) and Synapsin1A (D) in the brain of WT, ST3$^{-/-}$, WT 5XFAD, and ST3$^{-/-}$ 5XFAD mice. The brains of 8-month-old WT, ST3$^{-/-}$, WT 5XFAD, and ST3$^{-/-}$ 5XFAD mice were dissected after perfusion, mRNA was isolated and real-time RT PCR was performed as described in Materials and Methods. In A–D, means ± S. E. of 3–4 individual animals are shown (*, $p < 0.05$; ***, $p < 0.001$). (E, F) Comparison of cognitive abilities of 8-month-old WT, ST3$^{-/-}$, WT 5XFAD, and ST3$^{-/-}$ 5XFAD mice by Barnes maze test. Over a 4-day period, mice were trained to perform the task, and on day 5, the final trial was performed as described in Materials and Methods. The latency time was recorded during training on days 1–4 (E) and on the final trial on day 5 (F). In E, mean ± S.E. is shown for a group of 3–4 individual mice. In F, whisker plots with median and 10%/90% percentiles of 3–4 individual animals are shown (***, $p < 0.001$). Mean values are indicated by "+" symbols.

Gangliosides share the same structure and composition in all mammals from humans to rodents (Yu et al., 2011b). Therefore, in contrast to protein targets, which are often not structurally identical between mammalian species, the targeting of gangliosides can be modeled in mice or in in vitro model membrane systems. It was proposed that GM1 serves as a binding site for amyloid fragments to become a new center (seed) for aggregation (Yanagisawa, 2015; Yanagisawa et al., 1995). Another study conducted in a mouse model of AD confirmed that amyloid oligomeric peptides bind to neuronal GM1 in vivo, but was not clear whether and how such binding contributes to AD pathology (Hong et al., 2014). Studies that inhibited glucosylceramide synthase demonstrated that mouse cortical and hippocampal neurons become less susceptible to amyloid toxicity possibly by modulating expression of the insulin receptor, which is important for neuronal survival and functions (Herzer et al., 2016; Pomytkin et al., 2018). These studies suggested that the binding of amyloid fragments to gangliosides contributes to neurodegeneration and possibly to the progression of AD, but did not provide definitive proof in vivo.

Further in vitro studies on model membrane systems demonstrated that $A\beta_{1-40}$ peptides do not bind to isolated GM1 gangliosides but rather to rigid GM1 clusters in membrane domains stabilized by cholesterol (Kakio et al., 2001). These membrane domains with ganglioside clusters and cholesterol are known to be resistant to mild detergents such as 0.5% Triton X-100 and are referred to as lipid rafts. Experiments with model membranes with

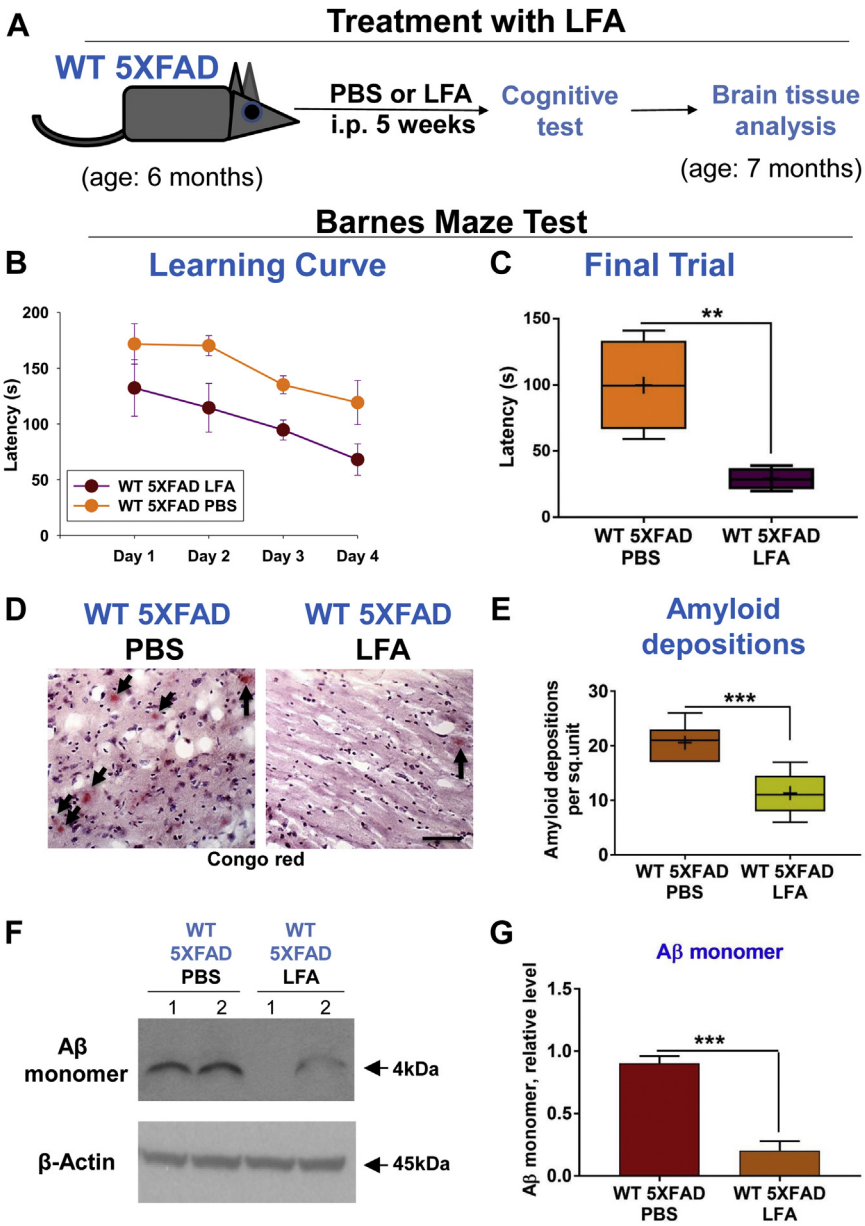

Fig. 8. Effects of administration of sialic acid–specific lectin LFA into 6-month-old WT 5XFAD mice for 5 weeks on cognitive abilities, the number of amyloid depositions, and Aβ monomers. (A) Scheme of systemic administration of LFA lectin (20 mg/kg) into 6-month-old WT 5XFAD mice 3 times a week for 5 weeks following Barnes maze test and analysis of brain cortex for signs of AD pathology. (B, C) Comparison of cognitive abilities of 7-month-old WT 5XFAD mice treated with PBS or LFA for 5 weeks before Barnes maze test. Over a 4-day period, mice were trained to perform the task and on day 5 a final trial was performed as for Fig. 7. The latency time was recorded during training on days 1–4 (B) and on the final trial on day 5 (C). (D) Comparison of images of the brain cortical area of PBS- versus LFA-treated WT 5xFAD mice. Brain sections were stained with Congo red to detect amyloid plaques as for Fig. 1 and representative images are shown. Amyloid depositions are indicated by arrows. Scale bar: 100 μm. (E) Quantification of amyloid plaque numbers in the brain cortical area of PBS- versus LFA-treated WT 5XFAD mice is shown. Quantification was performed as for Fig. 1. (F, G) Western blot analysis for Aβ monomer content in brains of 7-month-old WT 5XFAD treated for 5 weeks with PBS or LFA. For detection of 4 kDa Aβ monomer, 6E10 antibody was used and staining for β-actin was used as a loading control as for Fig. 2. Representative images are shown in F for 2 individual mice (labeled as 1 and 2). Quantitative analysis is shown in G. In B and G, mean ±S.E. is shown for the group of 4–5 individual mice (***, $p < 0.001$). In C and E, whisker plots with median and 10%/90% percentiles of 4–5 individual animals are shown (; **, $p < 0.01$; ***, $p < 0.001$). Mean values are indicated by "+" symbols. (For interpretation of the references to color in this figure legend, the reader is referred to the Web version of this article.)

modified GM1 demonstrated that amyloid peptide $A\beta_{1\text{-}40}$ binds efficiently to lyso-GM1, which lacks one fatty acid chain, indicating that the hydrophilic part of gangliosides is more important for binding than the fatty acid chain (Utsumi et al., 2009). In support of this, it was shown that binding of amyloid peptides $A\beta_{1\text{-}40}$ and $A\beta_{1\text{-}42}$ to asialo-GM1 was greatly reduced or completely inhibited (Ariga et al., 2001; Choo-Smith et al., 1997; Hong et al., 2014; Williamson et al., 2006). It was shown that $A\beta_{1\text{-}42}$ has a better ability to bind gangliosides than does less toxic $A\beta_{1\text{-}40}$ (Ariga et al., 2001), and the major brain poly-sialylated glycosphingolipids GQ1b, GT1b, and GD3 have a better ability to bind amyloid peptides than mono-sialylated GM1 or GD1a. These studies suggest a critical role for sialic acid connected to internal galactose on a carbohydrate core for amyloid peptide binding to major brain gangliosides; however, sialic acid connected to terminal galactose could also contribute to this binding (Ariga et al., 2001; Yu et al., 2011a). In support of this, treatment of primary cultured hippocampal neurons with neuraminidase that removes sialic acid from the surface of lipid rafts

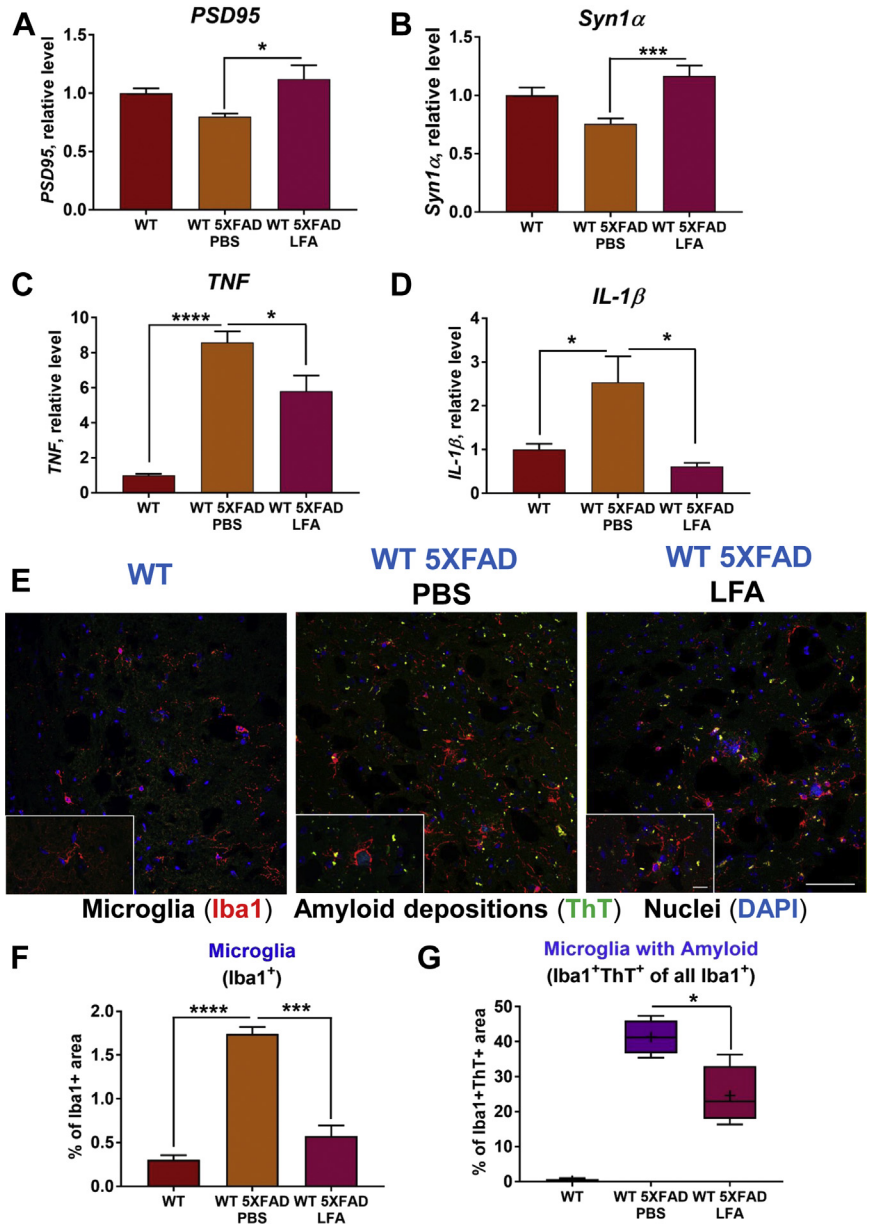

Fig. 9. Effect of administration of sialic acid–specific lectin LFA on the level of neuroinflammation and the expression of synaptic markers in WT 5XFAD mice. (A–D) Analysis of mRNA expression levels of synaptic markers PSD95 (A) and Syn1α (B), as well as proinflammatory cytokines TNF (C) and IL-1β (D) in the brains of PBS- versus LFA-treated 7-month-old WT 5XFAD mice. RNA isolation and real-time RT PCR was performed as for Fig. 7. (E–G) Brain histology sections of PBS- versus LFA-treated 7-month-old WT 5XFAD mice were prepared and stained for amyloid depositions with ThT-FITC (green), microglial cell marker Iba1 (red), and nuclear marker DAPI (blue) as in Fig. 2. Sites of colocalization of amyloid depositions and microglia (yellow color) are marked with arrows. Scale bars: 100 μm (lower magnification) and 10 μm (higher magnification). (F) Quantitative analysis of Iba1$^+$ microglial cell covered area in the brain cortical areas where amyloid depositions are evident. (G) Quantitative analysis of the percentage of Iba1$^+$microglia colocalized with ThT$^+$ amyloid depositions in the brain cortical areas where amyloid depositions are evident. In (A–D), means ± S. E. is shown for a group of 4–5 individual mice (*, $p < 0.05$; ***, $p < 0.001$; ****, $p < 0.0001$). In F and G, the analysis of sections from 3 animals with a total number of 15–20 section images is shown. Whisker plots with median and 10%/90% percentiles of 15–20 images are shown (*, $p < 0.05$; ***, $p < 0.001$; ****, $p < 0.0001$). Mean values are indicated by "+" symbols. (For interpretation of the references to color in this figure legend, the reader is referred to the Web version of this article.)

significantly decreased the level of neurotoxicity of $A\beta_{1-42}$ (Malchiodi-Albedi et al., 2010; Wang et al., 2001). Moreover, removal of the cholesterol that stabilizes neuronal lipid rafts also decreased amyloid-induced neurotoxicity (Wang et al., 2001). In addition, it was shown in acute hippocampal brain slice cultures that blocking the GM1 sialic acid with *Cholera* toxin subunit B decreases Aβ peptide oligomer-mediated LTP inhibition (Hong et al., 2014). These in vitro data demonstrate the importance of gangliosides within neuronal lipid rafts for the binding of amyloid fragments to neurons, which in turn causes neurotoxicity and decreases in neuronal synaptic activity.

Neuronal lipid rafts play an important role in normal and pathological CNS functions (Hicks et al., 2012; Simons and Ehehalt, 2002). In neurons, lipid rafts are present mostly in mature neurons in neurites and synapses and in the areas containing neurotrophic receptors such as TrkB (Tsui-Pierchala et al., 2002). Lipid rafts are also present in astroglial cells in the adult brain and are an integral part of structures of the blood-brain barrier (BBB) (Sotnikov et al., 2013). We have previously found that neuronal lipid rafts are directly recognized by platelets that become degranulated and produce a number of proinflammatory factors important for the development of autoimmune CNS inflammation (Ponomarev, 2018;

Sotnikov et al., 2013; Starossom et al., 2015). In AD pathology, glycolipid composition and the function of neuronal lipid rafts change as the disease progresses (reviewed by Yu et al., 2011a). It has been shown that in humans, GM1 and GM2 are accumulated in AD, whereas in 2XFAD mice with overexpression of hAPP/PS-1, there is an accumulation of GT1α, which have a high capacity to bind amyloid peptides (Ariga et al., 2001, 2010, 2013; Pernber et al., 2012). Our study indicates that the gangliosides GM1, GM2, GM3, GD1a, GD1b, GD2, GD3, GT1b, and GQ1b, which are absent in ST3$^{-/-}$ mice, play a key role in the development of AD pathology. However, ST3$^{-/-}$ mice still have gangliosides GM1b and GD1α (Yoshikawa et al., 2009; Yu et al., 2011b). In contrast to major brain gangliosides, GM1b and GD1α do not have internal galactose with sialic acid, which is critical for the binding of amyloid peptides (Ariga et al., 2001; Yu et al., 2011b). However, both GM1b and GD1α have terminal galactose with sialic acid, which contributes to the binding of amyloid peptides. Importantly, GD1α has sialic acid connected to GalNAc, which significantly enhances the binding of amyloid peptides (Ariga et al., 2001). Ganglioside GD1α is not expressed in WT mice, but it is found in ST3$^{-/-}$ mice (Yoshikawa et al., 2009). Thus, ST3$^{-/-}$ mice could still have binding sites for amyloid peptides, especially GD1α, which is the likely mediator of the residual AD pathology found in the ST3$^{-/-}$ 5XFAD mice in our study.

Two previous studies have investigated the role of particular gangliosides in vivo in mouse models of AD. The first study used mice lacking GM2-synthase that were crossed with 1XFAD mice that overexpress hAPP with Swedish and London mutations (Oikawa et al., 2009). These mice still express GD3, GM3, and GT3 but do not have GM1, GM2, GD1a, GD1b, GD2, GT1b, GQ1b, GM1b, or GD1α. Interestingly, GM2S$^{-/-}$ 1XFAD mice showed a significant increase in amyloid depositions in the CNS parenchyma and areas of CNS blood vessels with exacerbation of the disease (Oikawa et al., 2009). These results are not that surprising because these mice express GT3 and have a very high level of GD3 expression in blood vessels (Matsuda et al., 2006; Wen et al., 1999). The second study used GD3-synthase–deficient mice crossed with 2XFAD mice that overexpressed hAPP with a Swedish mutation and mutated human PS-1 gene. GD3S-deficient 2XFAD mice do not have GD2, GD3, GD1b, GT1b, or GQ1b but they have gangliosides GM1, GM2, GM3, and GD1a. Ganglioside analysis in the brain of these mice showed that the levels of GM1 and GD1a were significantly increased in these mice (Bernardo et al., 2009), whereas another study demonstrated an increase in GT1aα (Ariga et al., 2013). Similar to our ST3$^{-/-}$ 5XFAD mice that only had GM1b and GD1α, it was found that GD3S$^{-/-}$ 2XAPP mice had reduced levels of amyloid depositions and improved cognitive abilities (Bernardo et al., 2009). These results are quite surprising as GM1 has been shown in a number of in vivo and in vitro studies to be critical for Aβ binding (Yanagisawa, 2015). The observed decrease in AD pathology in these mice might be explained by a less robust model of AD in 2XFAD mice, which have 2 transgenes when compared with 5XFAD mice, which have 5 transgenes. Because GT1b and GQ1b have higher affinity to bind to Aβ than GM1 (Ariga et al., 2001), we could speculate that these gangliosides might play an important role in mouse models of AD along with GM1 and other a-series gangliosides such as GT1aα as it was reported in previous studies (Ariga et al., 2013; Bernardo et al., 2009). We believe that targeting a- and/or b-series gangliosides may be an effective AD therapy in the future.

It was reported that injection of *Vibrio cholera* sialidase that hydrolyzes complex b-series gangliosides to GM1 has a neuroprotective effect (Dhanushkodi and McDonald, 2011). It was also described that intracerebroventricular administration of isolated GM1 to patients with AD improved their condition (Svennerholm et al., 2002). Thus, the role of GM1 in AD pathology appeared to be complex. These contradictory results might be explained by the fact that amyloid depositions are formed on lipid rafts that contain many types of gangliosides and glycolipids besides GM1. The partial removal of sialic acid by *Vibrio cholera* sialidase or administration of naked GM1 could decrease binding of amyloid fragments to neuronal lipid frats. This is likely due to the removal of sialic acid by sialidase or competitive binding of amyloid fragments to administrated GM1.

To further verify the importance of targeting gangliosides in vivo, we treated WT 5XFAD mice with the sialic acid–specific lectin LFA. We observed that LFA, which specifically binds sialic acid regardless of its linkage to carbohydrates (Knibbs et al., 1993), was more potent in reducing the expression of proinflammatory cytokines TNF and IL-1β, which were not reduced in the ST3$^{-/-}$ 5XFAD mice. This is because LFA has broader specificity when compared with genetic elimination of gangliosides in ST3$^{-/-}$ mice that still express gangliosides GM1b and GD1α (Yoshikawa et al., 2009). We previously found that LFA effectively inhibited autoimmune neuroinflammation in a mouse model of experimental autoimmune encephalomyelitis, indicating its strong anti-inflammatory properties (Sotnikov et al., 2013). LFA has a molecular weight of 44 kDa and most likely do not pass intact BBB in healthy animals. However, in the brains of 5XFAD mice, BBB is disrupted especially at the sites of amyloid depositions (Kook et al., 2012). Thus, LFA has a potential double action to reduce amyloid depositions and inhibit AD-related neuroinflammation.

Microglia activation, infiltration of peripheral leukocytes, and upregulation of proinflammatory cytokines have been shown to be manifestations of AD-related neuroinflammation (Hansen et al., 2018; Heneka et al., 2015). Our studies in ST3$^{-/-}$ 5XFAD mice demonstrated that the level of microglia activation was reduced as determined by the expression of MHC class II and CD86. Infiltration of peripheral monocytes and lymphocytes was very low in WT 5XFAD mice, indicating the major role of microglia activation in this model. However, infiltration of peripheral leukocytes was still significantly reduced in ST3$^{-/-}$ FAD mice. Our findings also indicated that microglia in ST3$^{-/-}$ mice still underwent morphological changes of activation and were capable of amyloid phagocytosis. TNF was not reduced in ST3$^{-/-}$ mice and the expression of IL-1β was even elevated. Furthermore, our analysis of IL-1β expression in CD11b-positive cells of WT versus st3gal5-deficient mice demonstrated a comparable level of expression of this cytokine. This indicates that IL-1β is likely produced by other cell types such as astrocytes in ST3$^{-/-}$ 5XFAD mice. This hypothesis is in line with our earlier discovery that st3gal5-deficient animals have a higher level of astrocyte activation after injury (Dukhinova et al., 2018b). Thus, ST3$^{-/-}$ mice could have a complex phenotype, indicating a possible preference for other approaches besides genetic knockouts to target sialic acid in the brain of AD mice. We used for this purpose LFA, while other investigators successfully used sialidase NEU1 for AD treatment in a mouse model (Annunziata et al., 2013). The role of proinflammatory cytokines in AD pathology remains controversial. On the one hand, cytokine IL-1β contributes to AD pathology (Mariani et al., 2010). On the other hand, cytokine TNF has been shown to be beneficial in AD (Montgomery et al., 2011). Moreover, it was reported that IL-1β overexpression reduced amyloid plaque burden (Shaftel et al., 2007). Our results clearly show that ameliorated AD pathology is associated with a decrease in microglia activation markers MHC class II and CD86, but not proinflammatory cytokines, in ST3$^{-/-}$ mice. However, when we treated mice with LFA, TNF and IL-1β expression was reduced, as well as microglia activation. This implies that the extent of AD-related CNS inflammation is reduced when the disease is ameliorated.

Thus, our findings demonstrate the effectiveness of LFA treatment, which significantly decreased amyloid depositions in the

brain, possibly by binding to gangliosides in neuronal lipid rafts and preventing the binding of amyloid peptides. LFA treatment also inhibited neuroinflammation more effectively than deletion of the st3gal5 gene. It is clear that LFA is quite a broad-spectrum agent binding to sialic acid on different gangliosides and glycoproteins in the CNS and periphery. However, in the CNS, more than 80% of all glycans belong to glycolipids and 75% of sialic acid belongs to gangliosides (Schnaar et al., 2014). Thus, we believe that in our experiments, LFA mostly targeted brain gangliosides, reaching 80% of their targets in the brain. Although LFA does not demonstrate 100% specificity, we believe that our results highlight a very promising approach to specifically target sialylated brain-specific gangliosides such as GT1b or GQ1b that are expressed mostly in the brain. This approach has the potential to develop highly specific and efficient AD therapy in the future.

Disclosure

The authors declare no conflicts of interest.

Acknowledgements

This work was supported by a Research Grant Council-General Research Fund, Hong Kong grant, reference no. 14113316 (Hong Kong Government, Hong Kong), by a Research Grant Council–Areas of Excellence Fund grant (Hong Kong Government, Hong Kong), reference no. AoE/M-604/16, and by a Research Grant Council–Collaborative Research Fund grant (Hong Kong Government, Hong Kong), reference no. C6003-14G.

Appendix A. Supplementary data

Supplementary data to this article can be found online at https://doi.org/10.1016/j.neurobiolaging.2019.01.020.

References

Ando, S., 1983. Gangliosides in the nervous system. Neurochem. Int. 5, 507–537.
Annunziata, I., Patterson, A., Helton, D., Hu, H., Moshiach, S., Gomero, E., Nixon, R., d'Azzo, A., 2013. Lysosomal NEU1 deficiency affects amyloid precursor protein levels and amyloid-β secretion via deregulated lysosomal exocytosis. Nat. Commun. 4, 2734.
Ariga, T., Kobayashi, K., Hasegawa, A., Kiso, M., Ishida, H., Miyatake, T., 2001. Characterization of high-affinity binding between gangliosides and amyloid β-protein. Arch. Biochem. Biophys. 388, 225–230.
Ariga, T., Yanagisawa, M., Wakade, C., Ando, S., Buccafusco, J.J., McDonald, M.P., Yu, R.K., 2010. Ganglioside metabolism in a transgenic mouse model of Alzheimer's disease: expression of Chol-1α antigens in the brain. ASN Neuro 2, e00044.
Ariga, T., Itokazu, Y., McDonald, M.P., Hirabayashi, Y., Ando, S., Yu, R.K., 2013. Brain gangliosides of a transgenic mouse model of Alzheimer's disease with deficiency in GD3-synthase: expression of elevated levels of a cholinergic-specific ganglioside, Gt1aα. ASN Neuro. 5, 141–148.
Bernardo, A., Harrison, F.E., McCord, M., Zhao, J., Bruchey, A., Davies, S.S., Jackson Roberts, L., Mathews, P.M., Matsuoka, Y., Ariga, T., Yu, R.K., Thompson, R., McDonald, M.P., 2009. Elimination of GD3 synthase improves memory and reduces amyloid-β plaque load in transgenic mice. Neurobiol. Aging 30, 1777–1791.
Boza-Serrano, A., Yang, Y., Paulus, A., Deierborg, T., 2018. Innate immune alterations are elicited in microglial cells before plaque deposition in the Alzheimer's disease mouse model 5xFAD. Sci. Rep. 8, 1550.
Choo-Smith, L.P., Garzon-Rodriguez, W., Glabe, C.G., Surewicz, W.K., 1997. Acceleration of amyloid fibril formation by specific binding of Abeta-(1- 40) peptide to ganglioside-containing membrane vesicles. J. Biol. Chem. 272, 22987–22990.
Dhanushkodi, A., McDonald, M.P., 2011. Intracranial V. cholerae sialidase protects against excitotoxic neurodegeneration. PLoS One 6, e29285.
Dukhinova, M., Kopeikina, E., Ponomarev, E.D., 2018a. Usage of multiparameter flow cytometry to study microglia and macrophage heterogeneity in the central nervous system during neuroinflammation and neurodegeneration. Methods Mol. Biol. 1745, 167–177.
Dukhinova, M., Kuznetsova, I., Kopeikina, E., Veniaminova, E., Yung, A.W.Y., Veremeyko, T., Levchuk, K., Barteneva, N.S., Wing-Ho, K.K., Yung, W.H., Liu, J.Y.H., Rudd, J., Yau, S.S.Y., Anthony, D.C., Strekalova, T., Ponomarev, E.D., 2018b. Platelets mediate protective neuroinflammation and promote neuronal plasticity at the site of neuronal injury. Brain Behav. Immun. 74, 7–27.
Esiri, M.M., 2007. Ageing and the brain. J. Pathol. 211, 181–187.
Favaretto, A., Lazzarotto, A., Riccardi, A., Pravato, S., Margoni, M., Causin, F., Anglani, M.G., Seppi, D., Poggiali, D., Gallo, P., 2017. Enlarged Virchow Robin spaces associate with cognitive decline in multiple sclerosis. PLoS One 12, e0185626.
Fukami, Y., Ariga, T., Yamada, M., Yuki, N., 2017. Brain gangliosides in Alzheimer's disease: increased expression of cholinergic neuron-specific gangliosides. Curr. Alzheimer Res. 14, 586–591.
Graham, W.V., Bonito-Oliva, A., Sakmar, T.P., 2017. Update on Alzheimer's disease therapy and prevention strategies. Annu. Rev. Med. 68, 413–430.
Hansen, D.V., Hanson, J.E., Sheng, M., 2018. Microglia in Alzheimer's disease. J. Cell Biol. 217, 459–472.
Heneka, M.T., Carson, M.J., Khoury, J. El, Landreth, G.E., Brosseron, F., Feinstein, D.L., Jacobs, A.H., Wyss-Coray, T., Vitorica, J., Ransohoff, R.M., Herrup, K., Frautschy, S.A., Finsen, B., Brown, G.C., Verkhratsky, A., Yamanaka, K., Koistinaho, J., Latz, E., Halle, A., Petzold, G.C., Town, T., Morgan, D., Shinohara, M.L., Perry, V.H., Holmes, C., Bazan, N.G., Brooks, D.J., Hunot, S., Joseph, B., Deigendesch, N., Garaschuk, O., Boddeke, E., Dinarello, C.A., Breitner, J.C., Cole, G.M., Golenbock, D.T., Kummer, M.P., 2015. Neuroinflammation in Alzheimer's disease. Lancet Neurol. 14, 388–405.
Herzer, S., Meldner, S., Rehder, K., Gröne, H.J., Nordström, V., 2016. Lipid microdomain modification sustains neuronal viability in models of Alzheimer's disease. Acta Neuropathol. Commun. 4, 1–20.
Hicks, D.A., Nalivaeva, N.N., Turner, A.J., 2012. Lipid rafts and Alzheimer's disease: protein-lipid interactions and perturbation of signaling. Front. Physiol. 3, 189.
Hollmann, M., Seifert, W., 1986. Gangliosides modulate glutamate receptor binding in rat brain synaptic plasma membranes. Neurosci. Lett. 65, 133–138.
Hong, S., Ostaszewski, B.L., Yang, T., O'Malley, T.T., Jin, M., Yanagisawa, K., Li, S., Bartels, T., Selkoe, D.J., 2014. Soluble Aβ oligomers are rapidly sequestered from brain ISF in vivo and bind GM1 ganglioside on cellular membranes. Neuron 82, 308–319.
İzzetoğlu, S., Şahar, U., Şener, E., Deveci, R., 2014. Determination of sialic acids in immune system cells (coelomocytes) of sea urchin, Paracentrotus lividus, using capillary LC-ESI-MS/MS. Fish Shellfish Immunol. 36, 181–186.
Kakio, A., Nishimoto, S.I., Yanagisawa, K., Kozutsumi, Y., Matsuzaki, K., 2001. Cholesterol-dependent formation of GM1 ganglioside-bound amyloid β-protein, an endogenous seed for Alzheimer amyloid. J. Biol. Chem. 276, 24985–24990.
Knibbs, R.N., Osborne, S.E., Glick, G.D., Goldstein, I.J., 1993. Binding determinants of the sialic acid-specific lectin from the slug Limax flavus. J. Biol. Chem. 268, 18524–18531.
Kook, S.Y., Hong, H.S., Moon, M., Ha, C.M., Chang, S., Mook-Jung, I., 2012. A 1-42-RAGE interaction disrupts tight junctions of the blood-brain barrier via Ca2+-calcineurin signaling. J. Neurosci. 32, 8845–8854.
Landel, V., Baranger, K., Virard, I., Loriod, B., Khrestchatisky, M., Rivera, S., Benech, P., Féron, F., 2014. Temporal gene profiling of the 5XFAD transgenic mouse model highlights the importance of microglial activation in Alzheimer's disease. Mol. Neurodegener. 9, 33.
Lopez, P.H., Aja, S., Aoki, K., Seldin, M.M., Lei, X., Ronnett, G.V., Wong, G.W., Schnaar, R.L., 2017. Mice lacking sialyltransferase ST3Gal-II develop late-onset obesity and insulin resistance. Glycobiology 27, 129–139.
Malchiodi-Albedi, F., Contrusciere, V., Raggi, C., Fecchi, K., Rainaldi, G., Paradisi, S., Matteucci, A., Santini, M.T., Sargiacomo, M., Frank, C., Gaudiano, M.C., Diociaiuti, M., 2010. Lipid raft disruption protects mature neurons against amyloid oligomer toxicity. Biochim. Biophys. Acta 1802, 406–415.
Mariani, A., Cha, S.S., Bergstralh, E.J., Boardman, L.A., Dowdy, S.C., Keeney, G.L., Podratz, K.C., Melton, L.J., 2010. Referral and ascertainment bias in patients with synchronous and metachronous endometrial malignancy. Eur. J. Gynaecol. Oncol. 31, 5–9.
Masters, C.L., Bateman, R., Blennow, K., Rowe, C.C., Sperling, R.A., Cummings, J.L., 2015. Alzheimer's disease. Nat. Rev. Dis. Prim. 1, 15056.
Matsuda, J., Vanier, M.T., Popa, I., Portoukalian, J., Suzuki, K., 2006. GD3- and O-acetylated GD3-gangliosides in the GM2 synthase-deficient mouse brain and their immunohistochemical localization. Proc. Jpn. Acad. Ser. B Phys. Biol. Sci. 82, 189–196.
Mayo, L., Trauger, S.A., Blain, M., Nadeau, M., Patel, B., Alvarez, J.I., Mascanfroni, I.D., Yeste, A., Kivisäkk, P., Kallas, K., Ellezam, B., Bakshi, R., Prat, A., Antel, J.P., Weiner, H.L., Quintana, F.J., 2014. Regulation of astrocyte activation by glycolipids drives chronic CNS inflammation. Nat. Med. 20, 1147–1156.
Montgomery, S.L., Mastrangelo, M.A., Habib, D., Narrow, W.C., Knowlden, S.A., Wright, T.W., Bowers, W.J., 2011. Ablation of TNF-RI/RII expression in Alzheimer's disease mice leads to an unexpected enhancement of pathology: implications for chronic pan-TNF-α suppressive therapeutic strategies in the brain. Am. J. Pathol. 179, 2053–2070.
Oakley, H., Cole, S.L., Logan, S., Maus, E., Shao, P., Craft, J., Guillozet-Bongaarts, A., Ohno, M., Disterhoft, J., Van Eldik, L., Berry, R., Vassar, R., 2006. Intraneuronal beta-amyloid aggregates, neurodegeneration, and neuron loss in transgenic mice with five familial Alzheimer's disease mutations: potential factors in amyloid plaque formation. J. Neurosci. 26, 10129–10140.
Oikawa, N., Yamaguchi, H., Ogino, K., Taki, T., Yuyama, K., Yamamoto, N., Shin, R.W., Furukawa, K., Yanagisawa, K., 2009. Gangliosides determine the amyloid pathology of Alzheimer's disease. Neuroreport 20, 1043–1046.
Pavlov, D., Bettendorff, L., Gorlova, A., Olkhovik, A., Kalueff, A.V., Ponomarev, E.D., Inozemtsev, A., Chekhonin, V., Lesch, K.-P., Anthony, D.C., Strekalova, T., 2019.

Neuroinflammation and aberrant hippocampal plasticity in a mouse model of emotional stress evoked by exposure to ultrasound of alternating frequencies. Prog. Neuropsychopharmacol. Biol. Psychiatry 90, 104–116.
Pernber, Z., Blennow, K., Bogdanovic, N., Månsson, J.E., Blomqvist, M., 2012. Altered distribution of the gangliosides GM1 and GM2 in Alzheimer's disease. Dement. Geriatr. Cogn. Disord. 33, 174–188.
Pomytkin, I., Costa-Nunes, J.P., Kasatkin, V., Veniaminova, E., Demchenko, A., Lyundup, A., Lesch, K.P., Ponomarev, E.D., Strekalova, T., 2018. Insulin receptor in the brain: mechanisms of activation and the role in the CNS pathology and treatment. CNS Neurosci. Ther. 24, 763–774.
Ponomarev, E.D., 2018. Fresh evidence for platelets as neuronal and innate immune cells: their role in the activation, differentiation, and deactivation of Th1, Th17, and tregs during tissue inflammation. Front. Immunol. 9, 406.
Ponomarev, E.D., Tarasenko, T.N., Sapozhnikov, A.M., 2000. Splenic cytotoxic cells recognize surface HSP70 on culture-adapted EL-4 mouse lymphoma cells. Immunol. Lett. 74, 133–139.
Ponomarev, E.D., Shriver, L.P., Maresz, K., Dittel, B.N., 2005. Microglial cell activation and proliferation precedes the onset of CNS autoimmunity. J. Neurosci. Res. 81, 374–389.
Ponomarev, E.D., Veremeyko, T., Barteneva, N., Krichevsky, A.M., Weiner, H.L., 2011a. MicroRNA-124 promotes microglia quiescence and suppresses EAE by deactivating macrophages via the C/EBP-α-PU.1 pathway. Nat. Med. 17, 64–70.
Ponomarev, E.D., Veremeyko, T., Barteneva, N.S., 2011b. Visualization and quantitation of the expression of microRNAs and their target genes in neuroblastoma single cells using imaging cytometry. BMC Res. Notes 4, 517.
Posse de Chaves, E., Sipione, S., 2010. Sphingolipids and gangliosides of the nervous system in membrane function and dysfunction. FEBS Lett. 584, 1748–1759.
Rosenfeld, C.S., Ferguson, S.A., 2014. Barnes maze testing strategies with small and large rodent models. J. Vis. Exp. 26, e51194.
Schnaar, R.L., Gerardy-Schahn, R., Hildebrandt, H., 2014. Sialic acids in the brain: gangliosides and polysialic acid in nervous system development, stability, disease, and regeneration. Physiol. Rev. 94, 461–518.
Selkoe, D.J., Hardy, J., 2016. The amyloid hypothesis of Alzheimer's disease at 25 years. EMBO Mol. Med. 8, 595–608.
Shaftel, S.S., Kyrkanides, S., Olschowka, J.A., Miller, J.H., Johnson, R.E., O'Banion, M.K., 2007. Sustained hippocampal IL-1 beta overexpression mediates chronic neuroinflammation and ameliorates Alzheimer plaque pathology. J. Clin. Invest. 117, 1595–1604.
Shea, Y.F., Chu, L.W., Chan, A.O., Ha, J., Li, Y., Song, Y.Q., 2016. A systematic review of familial Alzheimer's disease: differences in presentation of clinical features among three mutated genes and potential ethnic differences. J. Formos. Med. Assoc. 115, 67–75.
Simons, K., Ehehalt, R., 2002. Cholesterol, lipid rafts, and disease. J. Clin. Invest. 110, 597–603.
Sotnikov, I., Veremeyko, T., Starossom, S.C., Barteneva, N., Weiner, H.L., Ponomarev, E.D., 2013. Platelets recognize brain-specific glycolipid structures, respond to neurovascular damage and promote neuroinflammation. PLoS One 8, e58979.
Soya, S., Şahar, U., Yıkılmaz, M., Karaçalı, S., 2017. Determination of sialic acids in the nervous system of silkworm (Bombyx mori L.): effects of aging and development. Arch. Biol. Sci. 69, 369–378.
Starossom, S.C., Veremeyko, T., Yung, A.W.Y., Dukhinova, M., Au, C., Lau, A.Y., Weiner, H.L., Ponomarev, E.D., 2015. Platelets play differential role during the initiation and progression of autoimmune neuroinflammation. Circ. Res. 117, 779–792.
Sturgill, E.R., Aoki, K., Lopez, P.H., Colacurcio, D., Vajn, K., Lorenzini, I., Majić, S., Yang, W.H., Heffer, M., Tiemeyer, M., Marth, J.D., Schnaar, R.L., 2012. Biosynthesis of the major brain gangliosides GD1a and GT1b. Glycobiology 22, 1289–1301.
Suzuki, T., Zhang, J., Miyazawa, S., Liu, Q., Farzan, M.R., Yao, W.D., 2011. Association of membrane rafts and postsynaptic density: proteomics, biochemical, and ultrastructural analyses. J. Neurochem. 119, 64–77.
Svennerholm, L., 1994. Chapter 30 Ganglioside loss is a primary event in Alzheimer disease Type I. Prog. Brain Res. 101, 391–404.
Svennerholm, L., Bråne, G., Karlsson, I., Lekman, A., Ramström, I., Wikkelsö, C., 2002. Alzheimer disease - effect of continuous intracerebroventricular treatment with GM1 ganglioside and a systematic activation programme. Dement. Geriatr. Cogn. Disord. 14, 128–136.
Tsui-Pierchala, B.A., Encinas, M., Milbrandt, J., Johnson, E.M., 2002. Lipid rafts in neuronal signaling and function. Trends Neurosci. 25, 412–417.
Utsumi, M., Yamaguchi, Y., Sasakawa, H., Yamamoto, N., Yanagisawa, K., Kato, K., 2009. Up-and-down topological mode of amyloid β-peptide lying on hydrophilic/hydrophobic interface of ganglioside clusters. Glycoconj. J. 26, 999–1006.
Vajn, K., Viljetić, B., Degmečić, I.V., Schnaar, R.L., Heffer, M., 2013. Differential distribution of major brain gangliosides in the adult mouse central nervous system. PLoS One 8, e75720.
Varki, A., 2008. Sialic acids in human health and disease. Trends Mol. Med. 14, 351–360.
Veremeyko, T., Starossom, S.C., Weiner, H.L., Ponomarev, E.D., 2012. Detection of microRNAs in microglia by real-time PCR in normal CNS and during neuroinflammation. J. Vis. Exp. 65, e4097.
Veremeyko, T., Kuznetsova, I.S., Dukhinova, M., Yung A, W.Y., Kopeikina, E., Barteneva, N.S., Ponomarev, E.D., 2018. Neuronal extracellular MicroRNAs miR-124 and miR-9 mediate cell-cell communication between neurons and microglia. J. Neurosci. Res. 97, 162–184.
Veremeyko, T., Yung, A., Anthony, D.C., Strekalova, T., Ponomarev, E.D., 2018a. Early growth response gene-2 is essential for M1 and M2 macrophage activation and plasticity by modulation of the transcription factor CEBPβ. Front. Immunol. 9, 2515.
Veremeyko, T., Yung, A.W.Y., Dukhinova, M., Kuznetsova, I.S., Pomytkin, I., Lyundup, A., Strekalova, T., Barteneva, N.S., Ponomarev, E.D., 2018b. Cyclic AMP pathway suppress autoimmune neuroinflammation by inhibiting functions of encephalitogenic CD4 T cells and enhancing M2 macrophage polarization at the site of inflammation. Front. Immunol. 9, 50.
Wang, S.S., Rymer, D.L., Good, T.A., 2001. Reduction in cholesterol and sialic acid content protects cells from the toxic effects of β-amyloid peptides. J. Biol. Chem. 276, 42027–42034.
Wen, F.Q., Jabbar, A.A., Patel, D.A., Kazarian, T., Valentino, L.A., 1999. Atherosclerotic aortic gangliosides enhance integrin-mediated platelet adhesion to collagen. Arterioscler. Thromb. Vasc. Biol. 19, 519–524.
Williamson, M.P., Suzuki, Y., Bourne, N.T., Asakura, T., 2006. Binding of amyloid β-peptide to ganglioside micelles is dependent on histidine-13. Biochem. J. 397, 483–490.
Yanagisawa, K., 2015. GM1 ganglioside and Alzheimer's disease. Glycoconj. J. 32, 87–91.
Yanagisawa, K., Odaka, A., Suzuki, N., Ihara, Y., 1995. GM1 ganglioside–bound amyloid β–protein (Aβ): a possible form of preamyloid in Alzheimer's disease. Nat. Med. 1, 1062–1066.
Yoshikawa, M., Go, S., Takasaki, K., Kakazu, Y., Ohashi, M., Nagafuku, M., Kabayama, K., Sekimoto, J., Suzuki, S. i., Takaiwa, K., Kimitsuki, T., Matsumoto, N., Komune, S., Kamei, D., Saito, M., Fujiwara, M., Iwasaki, K., Inokuchi, J. i., 2009. Mice lacking ganglioside GM3 synthase exhibit complete hearing loss due to selective degeneration of the organ of Corti. Proc. Natl. Acad. Sci. 106, 9483–9488.
Yu, R.K., Ariga, T., Wakade, C., 2011a. The pathological roles of ganglioside metabolism in Alzheimer's disease: effects of gangliosides on neurogenesis. Int. J. Alzheimers. Dis. 2011, 1–14.
Yu, R.K., Tsai, Y.-T., Ariga, T., Yanagisawa, M., 2011b. Structures, biosynthesis, and functions of gangliosides-an overview. J. Oleo Sci. 60, 537–544.
Zhang, X., Ding, L., Yang, L., Qin, W., Yuan, J., Li, S., Hu, W., 2016. Brain atrophy correlates with severe enlarged perivascular spaces in basal ganglia among lacunar stroke patients. PLoS One 11, e0149593.